Review in Black
Response in Red
Manuscript parts in blue

The manuscript of Wili et al. describes a very new and exciting experiment to measure dipolar couplings between two trityl radicals at Q-band frequencies using spin-lock techniques and phase modulation two pulse echo of this 'dressed spin states' in the nutation frame. This work adds a new possibilities to prolong the observation time window for the measurement of dipolar couplings in EPR which could be useful to extend the distance range in the future. Despite the fact that the experimental problems seen (and described very clear and fair in the manuscript) do not allow routine application of this methods yet for long distances (where the dipolar coupling strength is much less than the inhomogenous linewidth) this very new approach is very interesting.

The experiments as well as the theoretical description and discussion is very good, the literature is cited appropriately and the existing problems with this very new approach – especially limitations with respect to Rabi oscillation frequency strength in comparison with the inhomogeneous linewidth – is fair and clear described. There are many interesting aspects in this work, as for example also the large difference between T1rho and T2rho, which will stimulate further work in this direction. I recommend publication of this very nice and innovative article.

We are pleased to see your positive review.

Some small remarks:
- Line 26 there should be an 'for' instead of 'or'

We corrected the mistake (actually Line 24).

- The exchange interaction is explicitly mentioned in the theoretical part; also the fact that in the interaction frame it might gain some additional importance because the Zeeman splitting and the linewidth offsets disappear. But then it is not mentioned any more. Of course the two model systems will not show such contributions, but maybe the authors have investigated potential effects of this theoretically? It would be nice to have a remark on this aspect in the discussion (or conclusion). As far as I see all trityls will be in the strong coupling regime, so the method could also work for shorter distances, where such interaction might play a role.

We did not perform any simulations, but we now added a sentence in the theory part. The paragraph on the exchange coupling now reads (starting from line 124 in the highlighted manuscript);

If, both, the dressed spin offsets as well as the spin states of the two spins are the same, exchange coupling has no influence on the evolution. This is analogous to the situation of magnetically equivalent nuclei in liquid state NMR. This different averaging of dipolar and exchange contributions might be exploited experimentally to distinguish the two contributions.

- It will be interesting to see what happens with the deuterated trityl radicals. As mentioned this will be something for a new publication and might shine some more light on the big differences between T1rho and T2rho. Also the T dependence of these rotating frame relaxation rates could be very interesting (also to further optimize the experiment)
We agree that rotating frame relaxation in EPR is not very well understood and that additional studies are desirable. Unfortunately, we did not systematically investigate the T-dependence of T1rho and T2rho. We did look at temperature dependence of the decay of the spin-locked echo, but this cannot easily be

translated to T1rho and T2rho. (See also the answers we will provide to the Review of Jack Freed: https://doi.org/10.5194/mr-2020-7-RC2).
While the relaxation in dOTP is interesting as well, regarding application work, the important matrices are water/glycerol and lipid bilayers. The room-temperature rotating-frame relaxation times of (immobilized) trityls would be interesting as well.

- The exponential 'stretch' factors for the fits of T1rho and T2rho should also be given.

We now report them in all figure captions where they are relevant.

- The modulation amplitude aPM was set to 0.3 for the experiments and it is also mentioned in the manuscript that the theoretical modelling brakes down if this factor becomes too large. Can this be more quantified?

We did not systematically quantify this in a way that we could specify an exact cut-off where the experiment fails. We looked at the phase-pulse nutation curve (Fig. S5) and took a value where the dressed pi-pulse length was not too long, but the additional oscillations were not too large. Some articles (*e.g.* Laucht *et al.* https://journals.aps.org/prb/abstract/10.1103/PhysRevB.94.161302) point out that the breakdown of the rotating wave approximation could be used to generate faster switching times, i.e. pi pulses. So far, we do not see a reliable way of doing this. Note also that we use a phase-phase cycle, which should cancel some contributions from imperfect dressed spin pulses.

Review in Black
Response in Red
Manuscript parts in blue

The manuscript “Distance measurements between trityl radicals by pulse dressed electron paramagnetic resonance with phase modulation” by N. Wili, et al. describes a novel PDS method based on clever evolving dipolar coupling in the spin-locked state, thereby improving the distance range for trityl spin labels. The manuscript is generally correct and should be published with the consideration of the comments that we made.

This work describes an interesting development as so far it has not been demonstrated in ESR that spin-locked electron spins could be used to evolve selectively electron-electron dipolar coupling. The manuscript is well organized and clearly written. Also, extensive effort to synthesize and characterize rigid trityl biradicals and to simulate the evolution of coherence is shown. In particular, we like the implementation of the pulse sequence refocusing the nutation phase and providing the dipolar evolution sandwich in the locked state followed by the readout sequence, which can in principle exclude unwanted dipolar evolution. A simple two-pulse echo sequence used for readout appears sufficient at this stage, and by using SIFTER and DQC it would be possible to approach the somewhat shorter distance range. However, the dead-time cannot be excluded. Maybe the authors need to apply SIFTER or DQC sequences in the locked state.

We thank you for the generally positive comments. Regarding the dead time and other sequences in the locked state, you are correct. We added a comment in the manuscript, after the discussion of the pulse sequence (starting from line 241 in the highlighted manuscript):

If the dead time becomes too large for the relevant dipolar oscillations, one could, in principle, apply the known dead-time free single-frequency pulse sequences also as a phase-pulse sequence in the nutating frame.

It is encouraging that despite all the limitations imposed by the interaction strengths, the method does work and notably improves the dipolar evolution time for trityls. This work suggests a set of possible factors limiting T2(rho), and hopefully future work may be able to mitigate the effects of some of these factors. We doubt, however, that TWTA amplitude or phase noise contributes to shorter T2(rho). This is certainly not the case for amplitude noise, which within the locking bandwidth is estimated to be in the~1-10 mW range or maybe even less for a typical tube (less than -10 dBm/MHz noise spectral density). The phase noise of a TWTA (which is likely made by Applied System Engineering) is expected to be rather low. At least, the phase-noise test data for all amplifiers built over 20 years for ACERT supports this notion. Introducing phase noise, while possible, would be a complicated matter. AM/PM conversion in a saturated tube may be a possible way to test the effect on T1(rho) and T2(rho) to provide some insights on the instrumentation-imposed limits.

We thank you for the comments regarding the TWTA noise and sharing your experience with the noise figures. We based our comment on (Cohen et al. 2016: https://doi.org/10.1002/prop.201600071). (Which we now also clearly state in the manuscript). While we agree that the noise is rather small compared to the wanted driving field, it is not clear to us that one can safely conclude that it is irrelevant for T2rho. 10 mW is roughly a factor of 10000 smaller than the nominal 150 W nominal output power. This amounts to a factor of roughly 1% in terms of Rabi frequency, i.e. around 1 MHz. At least on first sight, it seems to be possible that this might contribute to T2rho.

Unfortunately, the work gives no clue regarding what to expect at a different temperature for T1(rho) and T2(rho). The experimental setup allows for easy temperature change and it is highly desirable to see the ratio of Tm/T2(rho) for at least one more temperature.

Under normal circumstances, we would simply measure it at another temperature and put the data in the SI. Unfortunately, with the current situation regarding COVID-19, we will be unable to provide these measurements in the coming months. We do not think that finalization of the paper should be held up that long.

The reason we did not measure at a different temperature so far is because we thought that a single additional temperature is not relevant. When comparing different temperatures, we also want to compare different matrices and measure rotating frame relaxation times at room temperature, i.e. for immobilized samples. Unfortunately, all of this must wait for the time being. It might also be too much for the scope of this manuscript. We do work on a more extended study on trityl relaxation.

At the beginning of the project we did measure decay of the spin-locked echo at different temperatures. However, as seen in Fig S3 of the submitted SI, this decay corresponds neither to T1rho nor to T2rho.

We hope that you still regard our proof-of-principle as relevant, although we measured only at a single temperature.

There is no comparison with the existing pulse sequences such as DQC or SIFTER,but we agree this may be unnecessary for this work. There is sufficient data in the literature for them, and PDS heavily relies on nitroxides anyway.

After emphasizing the power of major PDS methods in the introduction, the authors demonstrated that the sequence works at least for trityl labels, but they make no comment on whether it could be extended to any other known spin-label. The labels that are commonly used in biomedical research and are subjects of most of the key works cited are nitroxides, which demonstrate Tm's longer than the trityl's T2(rho) of this work. It is well known in this field that nitroxide labels quite often destabilize and precipitate proteins, the issue being even more critical with trityl labels, which are by no means mainstream. This is a significant limitation to the scope of this complex novel PDS method. Assuming that trityl labels were to have progressed to comparable use, there are other challenges that need to be addressed. The protein and lipid dynamics leading to Tm's in the low microsecond range as well as high local concentrations in the case of membrane proteins may contribute a set of problems in achieving T2ï ¿Aš anywhere close to that observed in this work in dOTP glass. Note that the T2(rho)'s obtained are considerably shorter than for nitroxides in this glass. We have (unpublished) data that demonstrate 40µs evolution time in this glass using the DEER-5 method; 4-pulse DEER is also not very far from this mark. We also found very long Tm's for (partly) deuterated proteins (Georgieva et al., J. Biol. Chem., 2010). We think this work should be cited in the context of deuterated proteins.

We stressed in the article that the Rabi frequencies must be larger than the offsets. This is of course not possible for most labels other than trityls with current hardware. We now emphasize more that nitroxides are the most commonly used labels and that there are cases where nitroxide Tm is longer than the T2rho that we observe for trityls.

Changes:

Introduction (line 63 in highlighted manuscript): “Note that the sequence presented in this work relies on the narrow spectrum of the trityl radicals. We do not expect it to work with the much more commonly used nitroxide radicals.”

Conclusion(line 415): “Note that in dOTP, the Tm values of the slow relaxing component of nitroxides (the relaxation of nitroxides in dOTP can be described by a sum of two stretched exponentials) can still be bigger than the T2rho times measured here for trityl radicals (Soetbeer2018).”

The mentioned paper by Georgieva et al. is now cited. We were unaware that it preceded the work by Ward et al. in 2010, and it is indeed relevant when discussing protein deuteration and PDS. We apologize for the oversight.

Regarding all the other issues: We agree that there are most likely other hurdles. Lipid dynamics might indeed contribute to shorter T2rho values – or it may not (some dynamics can indeed be decoupled in rotating frame experiments in NMR). Only experiment will tell. We publish our findings early to encourage other interested researchers to help answer these questions.

We clearly state in the conclusions that the sequence is not yet ready for application work. We believe that this statement is sufficiently strong in pointing out current limitations.

The special technical requirements of this experiment to provide long intense locking pulses need to be described in greater detail. Such pulses are not normally used in pulse ESR. A 150 W TWTA was employed to achieve~100 MHz Rabi frequency (36 G B1) and this power could last for about 40μs periods limited by the amplifier. In the first place it is a lot of power that can cause heating, arcing, and a damage to the receiver, thus limiting the repetition frequency. How was the receiver protected?

No special measures beyond the ones reported in (Doll & Jeschke, 2017) (now cited) were taken to protect the receiver – we simply made sure we had a spare switch and low-noise amplifier ready in case we destroy them. However, this has not happened so far (We started doing the experiments in August 2019). We also let it run overnight. We found no reduction in performance so far.

However, your point is now emphasized in the manuscript, in order to alert researchers who want to use this sequence or similar sequences that their hardware might be at risk.

We added the following paragraph in the Materials and Methods section (line 255):

Note that the long spin-lock pulses with full power can be dangerous for the receiver, since much of the power is reflected by the overcoupled resonator. We did not take any special measures beyond the receiver protection switch (Doll & Jeschke 2017). However, we are planning to install an additional limiter or a slow switch that could take more power. Since the spin-lock pulses are rather long, a slow switch could be used for most of the time, while the fast switch could be used for the transient times of the pulses to still provide the small dead time.

The origins of the baseline and of modulation depth need to be discussed.

We added the following lines in the results section:

Note that not only intermolecular dipolar couplings from remote spins contribute to the background. Transverse relaxation of dressed spins with time constant T2rho also contributes because we do not perform a constant time experiment. Regarding modulation depth we would have expected it to be unity, which is clearly not seen in our experiments. We suspect that imperfections in the dressed spin pi-pulse lead to an unmodulated background, which cannot be

removed by phase-cycling. The phenomenon is similar to reduced instantaneous diffusion for a Hahn Echo if the flip angle of the pi-pulse is reduced.

Figure S8 – legends need be corrected.

Thank you for pointing this out. We corrected the legend that was mixed up.

Distance measurement between trityl radicals by pulse dressed electron paramagnetic resonance with phase modulation

Nino Wili[1], Henrik Hintz[2], Agathe Vanas[1], Adelheid Godt[2], and Gunnar Jeschke[1]

[1]Department of Chemistry and Applied Biosciences, Laboratory of Physical Chemistry, ETH Zurich, Vladimir-Prelog-Weg 2, 8093 Zurich, Switzerland

[2]Faculty of Chemistry and Center for Molecular Materials (CM_2), Bielefeld University, Universitätsstrasse 25, 33615 Bielefeld, Germany

Correspondence: nino.wili@phys.chem.ethz.ch, https://orcid.org/0000-0003-4890-3842

Abstract.

Distance measurement in the nanometer range is among the most important applications of pulse electron paramagnetic resonance today, especially in biological applications. The longest distance that can be measured by all presently used pulse sequences is determined by the phase memory time T_m of the observed spins. Here we show that one can measure the dipolar coupling *during* strong microwave irradiation by using an appropriate frequency- or phase-modulation scheme, *i.e.* by applying pulse sequences in the nutating frame. This decouples the electron spins from the surrounding nuclear spins and thus leads to significantly longer relaxation times of the microwave-*dressed* spins (*i.e.* the rotating frame relaxation times $T_{1\rho}$ and $T_{2\rho}$) compared to T_m. The electron-electron dipolar coupling is not decoupled as long as both spins are excited, which can be implemented for trityl radicals at Q-band frequencies (35 GHz, 1.2 T). We show results for two bis-trityl rulers with inter-electron distances of about 4.1 nm and 5.3 nm and discuss technical challenges and possible next steps.

1 Introduction

Pulsed dipolar electron paramagnetic resonance (EPR) spectroscopy emerged as a powerful tool to measure distance distributions between electron spins in the nanometer range (Jeschke, 2012). This information is particularly useful when studying molecules and molecule assemblies that are intrinsically disordered or partially disordered or otherwise hard to crystallize and difficult to study with NMR or cryo-EM alone, *e.g.* certain membrane proteins (Bordignon and Bleicken, 2018) or protein-RNA complexes (Duss et al., 2014). The distance information is encoded in the magnetic dipole-dipole coupling between the electron spins, which depends on the inverse cubed distance, r^{-3}. A plethora of different techniques have been introduced, most notably double electron electron resonance (DEER) (Milov et al., 1984; Pannier et al., 2000), double quantum coherence (DQC) (Borbat and Freed, 1999), the single frequency for refocusing (SIFTER) (Jeschke et al., 2000), and relaxation induced dipolar modulation enhancement (RIDME) (Kulik et al., 2001; Milikisyants et al., 2009). The limiting factor for all these pulse sequences is the electron phase memory time T_m, which determines the maximal dipolar evolution time and thus the longest distance that can be measured. In many cases, the phase memory time can be prolonged by deuterating the solvent, or even the whole protein ~~(Ward et al., 2010; Schmidt et al., 2016)~~(Georgieva et al., 2010; Ward et al., 2010; Schmidt et al., 2016). How-

ever, such an approach is costly and is rarely feasible, *e.g.* it is very difficult for membrane proteins in a lipid bilayer and impossible ~~or~~ for in-cell work.

In recent years, several groups tried to use dynamical decoupling sequences based on multiple refocusing pulses (also known as Carr-Purcell sequences) in order to prolong the coherence times (Borbat et al., 2013; Spindler et al., 2015). Although shaped pulses significantly improved the fidelity of EPR experiments, pulse frequency band overlap and non-uniform inversion are still a problem in these sequences and can lead to artifacts, which may be corrected if traces with sufficient signal-to-noise and only moderately decaying background can be acquired (Breitgoff et al., 2017). Nevertheless, the improvements in T_m so far are on the order of a factor of 2, which only marginally (though sometimes decisively) improves the longest attainable distance.

Recently, a sequence based on spin-diffusion, which would be limited by T_1 rather than T_m, was proposed (Blank, 2017). This experiment is still waiting for experimental verification.

Here we propose a sequence where the longest dipolar evolution time is, in principle, limited by the rotating frame relaxation time $T_{2\rho}$, which is often much longer than T_m (for a discussion of $T_{2\rho}$ vs. the more familiar $T_{1\rho}$, *vide infra*). The complete dipolar evolution takes place *during* strong microwave irradiation. This decouples the electron spins from the surrounding nuclei (Jeschke and Schweiger, 1997) while the electron-electron coupling is still active. The spin manipulation during the strong microwave irradiation is achieved by short intervals of sinusoidal phase modulation. The frequency of this modulation needs to match the Rabi or nutation frequency of the spin-locking irradiation.

The latter approach was discovered more than once in the history of magnetic resonance. It traces back to investigations of Redfield on "rotary saturation" (Redfield, 1955). Hoult introduced the related idea of longitudinal field modulation for nutation frequency selective pulses to MRI (Hoult, 1979). Grzesiek and Bax picked up Hoult's idea, but used a phase modulation scheme instead and applied it to homonuclear mixing in solution state NMR (Grzesiek and Bax, 1995). They termed the technique "Audio-frequency NMR in a nutating frame", because their phase modulation (PM) frequency is in the audible range, and the pulse sequences effectively take place in a frame that nutates with the Rabi frequency of the spin-lock. Independently, Jeschke used longitudinal field modulation during a spin-lock for pulse EPR (Jeschke, 1999) and used the term "dressed EPR", because the spins are dressed by the microwave field during the spin-lock. This term is borrowed from quantum optics (Cohen-Tannoudji et al., 1992). The idea of dressed EPR originated in artifacts in hyperfine-decoupled electron-nuclear double resonance (ENDOR) spectra, which appear if the radio-frequency coil is not aligned perfectly perpendicular to the static field (Jeschke and Schweiger, 1997). Much later, it was also realized that field modulation should also prolong Rabi oscillations in the presence of inhomogeneous microwave fields (Saiko et al., 2018). Recently, the quantum information processing community picked up the idea of dressing electron spins in order to prolong coherence times (Laucht et al., 2016, 2017; Cohen et al., 2017). During the writing of this manuscript, Chen and Tycko came up with the idea of phase-modulation during a spin-lock independently again, and used it for slice selection during off-resonance spin-locks in solid-state, DNP-enhanced MRI (Chen and Tycko, 2020).

Here we combine the ideas of applying pulse sequences on dressed spins (Grzesiek and Bax, 1995; Jeschke, 1999) with the one of prolonging coherence times as a means of improving distance distribution resolution or prolonging distance range in pulsed dipolar EPR spectroscopy. To test the method, we used two bis-trityl rulers in which two trityl radicals are connected by

a rather stiff linker. Linker length and residual flexibility are known (Godt et al., 2006; Jeschke et al., 2010). The chosen trityl radical is structurally closely related to the Finland trityl radical and has similar EPR spectroscopic properties (Hintz et al., 2019). The narrow EPR spectrum of the used trityl radical makes it particularly amenable to single-frequency techniques for measurements of the dipole-dipole coupling (Reginsson et al., 2012) in a regime that is analogous to the one of homonuclear NMR experiments. Note that the sequence presented in this work relies on the narrow spectrum of the trityl radicals. We do not expect it to work with the much more commonly used nitroxide radicals.

The article is organized as follows: First, we review mathematically, in the language of the magnetic resonance community, what happens to all the interactions in the spin Hamiltonian if we apply a strong microwave field. In order to do this, we will introduce a nutating frame description. Then we explain how an appropriate phase modulation scheme leads to "pulses" in the nutating frame. In the results section we show the synthesis of the bis-trityl rulers and present the application of a dressed spin echo experiment to such rulers to measure the dipolar coupling between two trityl radicals.

2 Theory

We use the following convention for operators: No prime refers to the laboratory frame and one prime to the electron-spin rotating frame, *i.e.* the interaction frame with the Zeeman Hamiltonian of the electrons. Two primes refer to the nutating frame, which is obtained with an additional interaction frame transformation with the pulse Hamiltonian. We will usually only denote the Hamiltonian with primes, and not all operators. If we mention axes in the text, we will explicitly use the primes, but we will omit them in mathematical formulas.

2.1 Averaging of interactions by strong continuous microwave irradiation

In order to understand the observations in this work, we need to study the influence of strong microwave irradiation on the different interactions present in the spin system. The spin Hamiltonian of a system with two coupled electrons ($S = 1/2$) in a bath of nuclei is given in the rotating frame by

$$\hat{\mathcal{H}}' = \hat{\mathcal{H}}'_{\text{mw}} + \hat{\mathcal{H}}'_{\text{offset}} + \hat{\mathcal{H}}'_{\text{e-e}} + \hat{\mathcal{H}}'_{\text{e-n}} + \hat{\mathcal{H}}'_{\text{nuc}} \quad . \tag{1}$$

The first term is the microwave Hamiltonian, which is given in the electron-spin rotating frame by

$$\hat{\mathcal{H}}'_{\text{mw}} = \omega_1 \left(\hat{S}_{1,x} + \hat{S}_{2,x} \right) \text{ with } \omega_1 = -\gamma_e B_1 \quad . \tag{2}$$

The Rabi or nutation frequency is denoted by ω_1, which depends on the microwave amplitude B_1 and the gyromagnetic ratio of the electron, γ_e. We assume a constant microwave phase and neglect the influence of the microwaves on the nuclear spins. In the following, we will apply an interaction frame transformation (IAT) with $\hat{\mathcal{H}}'_{\text{mw}}$ to all other terms and use first-order average Hamiltonian theory to gain physical insight. The new frame is referred to as the nutating frame. The nutating frame Hamiltonian is based on spin operators for dressed electron spins and bare nuclear spins. For mathematical details please consult the SI.

If we choose the nutating frame frequency ω_{PM} equal to the Rabi frequency, $\omega_{\text{PM}} = \omega_1$, the irradiation term is completely absorbed into the frame. In a real experiment with an ensemble of spins, ω_1 will be distributed due to microwave inhomogeneities,

thus we will always have a remaining contribution of

$$\hat{\mathcal{H}}''_{\text{mw}} = \Omega_{\text{d}} \left(\hat{S}_{1,x} + \hat{S}_{2,x} \right) \text{ with } \Omega_{\text{d}} = (\omega_1 - \omega_{\text{PM}}) \quad . \tag{3}$$

The dressed spin offset Ω_{d} will be distributed over the sample, but as a molecule is by orders of magnitude smaller than the microwave wavelength, Ω_{d} will be the same for all electron spins within one molecule.

As usual, the influence of a small g-anisotropy and of an inhomogeneous static magnetic field B_0 is captured in offset terms in the rotating frame

$$\hat{\mathcal{H}}'_{\text{offset}} = \Omega_{S,1} \hat{S}_{1z} + \Omega_{S,2} \hat{S}_{2z} \quad . \tag{4}$$

We neglect any tilt of the electron spin quantization axis due to strong g-anisotropy, which is a good approximation for trityl and other organic radicals. The first-order average Hamiltonian after an IAT with $\hat{\mathcal{H}}'_{\text{mw}}$ vanishes, *i.e.*

$$\hat{\mathcal{H}}''_{\text{offset}} = 0 \quad . \tag{5}$$

In pulse EPR, the spectral width is often much larger than the Rabi frequency. In this case, the first order approximation will be poor. It is, however, not a poor approximation for trityl radicals with our setup. For simplicity, we will mostly neglect the effect of resonance offsets $\Omega_{S,1}$ and $\Omega_{S,2}$.

The most important term in the context of distance measurements is the electron-electron coupling Hamiltonian, which contains dipolar and exchange (J) contributions

$$\begin{aligned}
&\hat{\mathcal{H}}'_{\text{e-e}} = \hat{\mathcal{H}}'_{\text{e-e,dip}} + \hat{\mathcal{H}}'_{\text{e-e,J}} \\
&\hat{\mathcal{H}}'_{\text{e-e,dip}} = \omega_{\text{dd}} \left(\hat{S}_{1z} \hat{S}_{2z} - \frac{1}{2} \left(\hat{S}_{1x} \hat{S}_{2x} + \hat{S}_{1y} \hat{S}_{2y} \right) \right) \\
&\omega_{\text{dd}} = \frac{\mu_0}{4\pi} \frac{\mu_{\text{B}}^2 g_1 g_2}{\hbar} \frac{1}{r_{12}^3} \left(1 - 3\cos^2\theta \right) \\
&\hat{\mathcal{H}}'_{\text{e-e,J}} = J \left(\hat{\boldsymbol{S}}_{\mathbf{1}} \cdot \hat{\boldsymbol{S}}_{\mathbf{2}} \right)
\end{aligned} \tag{6}$$

where μ_0 is the vacuum permeability, μ_{B} the Bohr magneton, g_1 and g_2 are the g-factors of the two electron spins, and θ is the angle between the external magnetic field and the interspin vector with length r_{12}. The exchange contribution is often, but not always negligible in pulse EPR based distance measurements. The prefactor of the dipolar coupling contains the distance information and is given by

$$d = \frac{1}{2\pi} \frac{\mu_0}{4\pi} \frac{\mu_{\text{B}}^2 g^2}{\hbar} \frac{1}{r^3} \quad . \tag{7}$$

This amounts to 52.04 MHz for $r = 1$ nm. After transformation to the nutating frame, we obtain

$$\begin{aligned}
&\hat{\mathcal{H}}''_{\text{e-e,dip}} = -\frac{1}{2} \cdot \omega_{\text{dd}} \left(\hat{S}_{1x} \hat{S}_{2x} - \frac{1}{2} \left(\hat{S}_{1z} \hat{S}_{2z} + \hat{S}_{1y} \hat{S}_{2y} \right) \right) \\
&\hat{\mathcal{H}}''_{\text{e-e,J}} = \hat{\mathcal{H}}'_{\text{e-e,J}} = J \left(\hat{\boldsymbol{S}}_{\mathbf{1}} \cdot \hat{\boldsymbol{S}}_{\mathbf{2}} \right) \quad .
\end{aligned} \tag{8}$$

The electron-electron dipolar coupling is not averaged to zero, but only scaled by a factor of -1/2. It is also tilted such that the unique axis of the coupling Hamiltonian points along the spin-lock axis ($z' \rightarrow x'' = x'$, in the NMR literature, often a tilted frame is used). In other words, the two dressed spins are still dipole-dipole coupled with half the original coupling strength and with inverted sign of the interaction. This result is well-known in solid-state NMR (Rhim et al., 1970), where it is used to generate "magic echoes". The isotropic J-coupling is unaffected if both spins are irradiated. Note however that the difference of the resonance frequencies of the two dressed spins is much smaller than the one of the bare spins, as remarked upon already by Grzesiek and Bax (Grzesiek and Bax, 1995). The difference in relative magnitude of the exchange coupling and resonance frequency difference can lead to a different manifestation of the exchange coupling in the spectra. If, both, the dressed spin offsets as well as the spin states of the two spins are the same, exchange coupling has no influence on the evolution. This is analogous to the situation of magnetically equivalent nuclei in liquid state NMR. This different averaging of dipolar and exchange contributions might be exploited experimentally to distinguish the two contributions.

The term $\hat{\mathcal{H}}'_{\text{e-n}}$ contains all electron-nucleus (hyperfine) couplings. If the Rabi frequency of the irradiation is much larger than all hyperfine couplings and nuclear Zeeman frequencies, this term also averages to zero in the nutating frame, *i.e.*

$$\hat{\mathcal{H}}''_{\text{e-n}} = 0 \quad , \tag{9}$$

an effect referred to as hyperfine decoupling (Jeschke and Schweiger, 1997). Terms that do not contain an electron spin operator are assumed to be unaffected by the microwave irradiation,

$$\hat{\mathcal{H}}_{\text{nuc}} = \hat{\mathcal{H}}'_{\text{nuc}} = \hat{\mathcal{H}}''_{\text{nuc}} \quad . \tag{10}$$

Equations (9) and (10) might appear to be irrelevant to distance measurements between electrons, but they are not. The terms $\hat{\mathcal{H}}_{\text{e-n}}$ and $\hat{\mathcal{H}}_{\text{nuc}}$ do not commute if nuclear-nuclear flip-flop terms are present, even if the hyperfine coupling $\hat{\mathcal{H}}_{\text{e-n}}$ is purely secular (no electron spin echo envelope modulation effect). For example, for the flip-flop terms in $\hat{\mathcal{H}}_{\text{nuc}}$, $\left[\hat{S}_z\hat{I}_{iz}, \hat{I}_i^+\hat{I}_j^-\right] \neq 0$. A simple spin echo sequence on the electron spins thus does *not* completely refocus the hyperfine coupling - the result is a dephasing of the electron spins, sometimes loosely referred to as "relaxation". In principle, this dephasing stems from coherent evolution, but since the nuclear spin bath is usually very large, it is computationally very expensive to simulate a real system. Accordingly, most theoretical studies treat the internuclear couplings phenomenologically using effective flip rates (Klauder and Anderson, 1962). The situation during microwave irradiation of an electron-nuclear spin system has many parallels with heteronuclear decoupling in solid-state NMR (Ernst, 2003), where one distinguishes between the "real" transverse relaxation time due to incoherent dynamics, T_2, and the effective relaxation time that is measured with a spin echo, T_2' and has large coherent contributions. Of course, in EPR, the coupling strengths and Rabi frequencies are several orders of magnitude higher than in NMR.

In EPR measurements of organic radicals at sufficiently low temperatures, usually at 50 K and below, the hyperfine and nuclear-nuclear couplings dominate the dephasing (Brown, 1979). In this case, averaging the hyperfine coupling to zero should drastically increase the dephasing time, because $\hat{\mathcal{H}}_{\text{nuc}}$ commutes with all remaining terms containing electron spin operators. At the same time, according to Eq. (8), the effective dipolar coupling is scaled by a factor -1/2. If the gain in dephasing time

is larger than a factor of two, it should - in principle - be possible to measure longer dipolar dephasing traces and thus longer distances. As we shall see later, the effective scaling factor may be even more favourable (-3/4), as the flip-flop terms in the electron-electron dipolar Hamiltonian may be truncated for bare spins but can be significant for dressed spins.

The immediate next question is then how one can measure the dipolar coupling during a spin-lock pulse. We propose to use a phase-modulation scheme that we discuss in the next section.

2.2 Pulse dressed spin resonance with phase-modulated pulses

The basic theory of dressed spin resonance is already described in (Grzesiek and Bax, 1995) and (Jeschke, 1999) but we describe it here again for completeness and consistency.

For simplicity and illustration, we first look at an isolated electron (spin 1/2) in a static magnetic field B_0 along the laboratory-frame z-axis. If we irradiate this system with a linearly polarized electromagnetic field with frequency ω_{mw} and amplitude $2B_1$, the Hamiltonian in angular frequency units is given by

$$\hat{\mathcal{H}} = \omega_0 \hat{S}_z + 2\omega_1 \cos\left(\omega_{\mathrm{mw}} t + \phi_{\mathrm{mw}}(t)\right) \hat{S}_x, \tag{11}$$

with $\omega_0 = -\gamma B_0$. We include an arbitrary phase $\phi_{\mathrm{mw}}(t)$, which we will use later to generate dressed spin PM pulse sequences. As usual, we now go into a rotating frame with frequency ω_{mw}. If we neglect the time-dependent terms (rotating wave approximation, RWA), we obtain

$$\hat{\mathcal{H}}' = \Omega_S \hat{S}_z + \omega_1 \left(\cos\left(\phi_{\mathrm{mw}}(t)\right) \hat{S}_x + \sin\left(\phi_{\mathrm{mw}}(t)\right) \hat{S}_y \right), \tag{12}$$

with the offset $\Omega_S = (\omega_0 - \omega_{\mathrm{mw}})$, which is also used in Eq. (4). The main effect of the time-dependent terms is a Bloch-Siegert shift, *i.e.* just a small correction of Ω_S. We can choose the PM as

$$\phi_{\mathrm{mw}}(t) = \phi_0 + a_{\mathrm{PM}} \cos\left(\omega_{\mathrm{PM}} t + \phi_{\mathrm{PM}}\right), \tag{13}$$

with a modulation amplitude a_{PM}, a modulation frequency ω_{PM} and a modulation phase ϕ_{PM}. The phase ϕ_0 is what one would conventionally call the phase of the microwave pulse applied to the bare spins, *i.e.* $[0, \pi/2, \pi, 3\pi/2]$ for $[x, y, -x, -y]$. Likewise, ϕ_{PM} is the phase of the PM pulse that is applied to the dressed spins. We use $\phi_0 = 0$ for the following discussion. For small modulation amplitudes, $a_{\mathrm{PM}} \ll 1$, we can use the approximations $\cos(\phi_{\mathrm{mw}}) \approx 1$ and $\sin(\phi_{\mathrm{mw}}) \approx \phi_{\mathrm{mw}}$ and obtain a truncated rotating-frame Hamiltonian

$$\hat{\mathcal{H}}' \approx \Omega_S \hat{S}_z + \omega_1 \hat{S}_x + \omega_1 a_{\mathrm{PM}} \cos\left(\omega_{\mathrm{PM}} t + \phi_{\mathrm{PM}}\right) \hat{S}_y. \tag{14}$$

For a hard pulse, *i.e.* $\omega_1 \gg \Omega_S$, we can now apply a second interaction frame transformation with $\omega_{\mathrm{PM}} \hat{S}_{x'}$, use the RWA again, and obtain the dressed rotating frame Hamiltonian

$$\hat{\mathcal{H}}'' = \Omega_{\mathrm{d}} \hat{S}_x + \frac{\omega_1 a_{\mathrm{PM}}}{2} \left(\cos\left(\phi_{\mathrm{PM}}\right) \hat{S}_y + \sin\left(\phi_{\mathrm{PM}}\right) \hat{S}_z \right) \quad , \tag{15}$$

with the dressed spin offset $\Omega_\mathrm{d} = (\omega_1 - \omega_\mathrm{PM})$, already introduced in Eq. (3), and a dressed spin nutation (Rabi) frequency of $\omega_1 a_\mathrm{PM}/2$. Again, the RWA implies that we neglect a Bloch-Siegert shift, now for the dressed spins, which would introduce a correction to Ω_d. The whole situation is analogous to the rotating frame Hamiltonian in Eq. 12, but with an exchange of axes.

Some words of caution: First, in EPR unlike in NMR, the hard pulse limit will often not be fulfilled. In a first step, one can use an interaction frame transformation with the whole effective nutation field, $\Omega_S \hat{S}_z + \omega_1 \hat{S}_x$. For the sake of intuitive clarity, we will not do this for the qualitative discussion. Second, one can easily choose a large a_PM, such that the RWA leading from Eq. (14) to Eq. (15) is seriously invalid. This was recognized already in (Grzesiek and Bax, 1995), and studied separately in (Laucht et al., 2016). In our study, imperfection of the RWA is visible in nutation curves, but the final results do not seem to be affected. The problem might be alleviated by using an appropriate frequency or amplitude modulation in order to generate a circularly polarized field in the rotating frame.

There are two alternatives to the phase-modulation schemes. One could equivalently formulate the dressed spin resonance as a frequency-modulation. Phase- and frequency modulation are physically equivalent, but we prefer the phase-modulation because the description of frequency-modulation involves a time-dependent offset/detuning and thus a "wobbling" frame, which makes it harder to keep track of relative phases of coherences. Instead of any microwave/radio-frequency modulation, one could also use a modulation of the magnetic field along the laboratory frame z direction (Jeschke, 1999). Depending on the setup, the relative phase of the modulation can be locked to the phase of the driving field or not. If an arbitrary waveform generator setup is available, phase modulation may be preferable, as it does not require modulation coils and a radiofrequency amplifier and makes synchronization of bare-spin and dressed-spin pulses much easier. However, the amplitude of the phase pulses depend on the Rabi frequency itself in the case of phase modulation. By using an external oscillating field, this dependence would vanish.

2.3 Pulse sequence

The pulse sequence used to measure the dipolar coupling in this work is the dressed-spin primary echo sequence shown in Fig. 1. It can be readily understood with results from the previous sections. For dipolar measurements, one chooses $\tau_1 = \tau_2$ and constant T_SL. The first $\pi/2$ pulse generates electron coherence. Since we deal with trityl radicals, the excitation can be nearly uniform on our setup. The spins are then locked with a spin-lock pulse that is 90 degrees phase shifted with respect to the first pulse. Let us assume that the spin-lock and the coherences are along x'. For free dressed-spin evolution, *i.e.* in the absence of phase modulation, we can assume the following Hamiltonian during the spin-lock in the nutating frame:

$$\begin{aligned}\hat{\mathcal{H}}'' = {} & \Omega_\mathrm{d} \left(\hat{S}_{1x} + \hat{S}_{2x} \right) \\ & - \frac{\omega_\mathrm{dd}}{2} \left(\hat{S}_{1x}\hat{S}_{2x} - \frac{1}{2} \left(\hat{S}_{1z}\hat{S}_{2z} + \hat{S}_{1y}\hat{S}_{2y} \right) \right),\end{aligned} \tag{16}$$

where we recall that $\Omega_\mathrm{d} = (\omega_1 - \omega_\mathrm{PM})$. Note that ω_1 is inhomogeneous over the sample, but is the same within each pair of spins.

The Hamiltonian in Eq. 16 is analogous to the one in the rotating frame, but to a very good approximation the offsets are the same for both dressed electron spins. Additionally, all hyperfine couplings vanish. The phase modulation pulses act on the

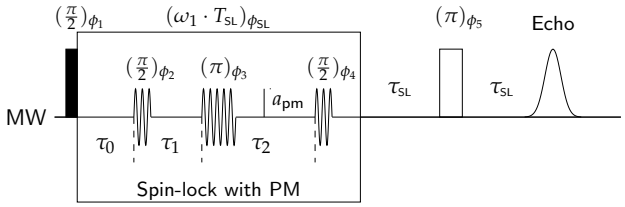

Figure 1. Pulse sequence used to measure the dipolar coupling during a spin-lock. Note that $|\phi_{SL} - \phi_1| = \pi/2$. The phases ϕ_{2-4} correspond to ϕ_{PM} in Eq. 13, while $\phi_{SL} = \phi_0$ in the same equation. Details for the inner working of the sequence are given in the main text.

dressed spins in the nutating frame. We can thus generate a *dressed spin echo* by a phase-pulse sequence $\pi/2-t-\pi-t$. A third $\pi/2$ pulse is needed that rotates any refocused dressed-spin coherence back to the $x'' = x'$ axis. The magnetization resulting from this backrotation is locked again, until it is detected by the remaining $\tau-\pi-\tau-$ echo sequence. A very similar sequence was already demonstrated with z-modulation pulses in (Jeschke, 1999), albeit not for dipole-dipole coupled electron spins.

The dressed-spin echo is needed to refocus microwave field inhomogeneities (*i.e.* a distribution of ω_1 and thus also Ω_d). The dipolar part of the Hamiltonian is unaffected by the PM-π pulse, because this pulse inverts both spin operators at the same time. With effects of the other terms being refocused, it is sufficient to only keep the dipolar part during the periods τ_1 and τ_2:

$$\tilde{\hat{\mathcal{H}}}'' = -\frac{\omega_{dd}}{2}\left(\hat{S}_{1x}\hat{S}_{2x} - \frac{1}{2}\left(\hat{S}_{1z}\hat{S}_{2z} + \hat{S}_{1y}\hat{S}_{2y}\right)\right). \tag{17}$$

At the start of the period τ_1, the system is in the state $\hat{\sigma}'' = \hat{S}_{1z} + \hat{S}_{1z}$ (or along y'', depending on the phase ϕ_2). For $\tau_1 = \tau_2$, this evolves according to

$$\begin{aligned}\hat{\sigma}'' \xrightarrow{\tilde{\hat{\mathcal{H}}}''\cdot 2\tau_1} &\cos\left(\frac{3}{4}\omega_{dd}\tau_1\right)\left(\hat{S}_{1z} + \hat{S}_{1z}\right) \\ &+ \sin\left(\frac{3}{4}\omega_{dd}\tau_1\right)\left(2\hat{S}_{1x}\hat{S}_{1y} + 2\hat{S}_{1y}\hat{S}_{1x}\right) \quad .\end{aligned} \tag{18}$$

The z'' terms are then flipped to $x'' = x'$, are transferred to bare-spin coherence at the end of the microwave pulse and are then detected by the echo. The other terms do not contribute to the detected signal. The factor of $3/4$ has two contributions. A factor of $(-)1/2$ is due to the spin-lock and the partial averaging of the dipolar coupling, see Eq. (8). A factor of $3/2$ is due to the strong coupling regime in the dressed frame, because the dressed electron spins are equivalent. This scaling by a factor of $3/2$ for trityl biradicals has been observed before at short distances with established single-frequency techniques (Meyer et al., 2018), where it results from the dipole-dipole coupling being much larger than the mean difference of the resonance frequencies of two trityl radicals. In conclusion, we expect that for dressed spins echo intensity oscillates with $3/4$ of the dipolar coupling, which for a fixed or narrowly distributed distance will manifest in a Pake pattern because the measurements are conducted in frozen solution.

The timing τ_{SL} of the read-out echo does, in principle, affect the resulting dipolar spectrum, because it acts as filter with the signal intensity scaling with $\cos\omega_{dd}\tau_{SL}$. However, for short interpulse delays and long distances, such filtering should be

negligible. If necessary, a SIFTER-type readout sequence could be used, which refocuses both the offsets and the dipolar couplings.

It is noteworthy that, in principle, a normal two-pulse echo on the bare spins with non-selective pulses would be sufficient to measure the dipolar coupling. In practice, this approach is usually much inferior to the DQC and SIFTER sequences, because the phase memory time is of the same order of magnitude as the dipolar oscillations, echo decay is not monoexponential and contains other contributions, and dead-time is significant. The combination of these complications makes it very difficult to separate the dipolar oscillation. Under the spin-lock, the relaxation is sufficiently slowed down, such that the dipolar evolution is clearly distinguishable, and the dead time in a PM-pulse sequence is nearly zero. If the dead time becomes too large for the relevant dipolar oscillations, one could, in principle, apply the known dead-time free single-frequency pulse sequences DQC and SIFTER also as a phase-pulse sequence in the nutating frame.

2.4 Expected limitations

The derivation of the modulation formula in Eq. (18) depends on the condition that ω_1 is much bigger than all other frequencies present in the system. Especially for the bare-spin resonance offsets, this approximation is not fulfilled very well. In principle, one could account for the different offsets analytically, but this is rather tedious and does not provide much additional insight. We will present numerical simulations in the result section to illustrate the deviations.

3 Materials and methods

All measurements were performed on a home-built Q-band spectrometer equipped with a Keysight M8190A arbitrary waveform generator operating at 8 GS/s and an ADC with a sampling frequency of 2 GHz (SP Devices ADQ412) (Doll, 2016). The highly flexible software made it straightforward to implement the pulse sequences with PM pulses, in contrast to commercial analogues. Microwave pulses were amplified with a travelling wave tube (TWT) amplifier with 150 W nominal output power (Applied Systems Engineering). A home-built Q-band loop-gap resonator for 1.6 mm tubes was used (Tschaggelar et al., 2017). Note that the long spin-lock pulses with full power can be dangerous for the receiver, since much of the power is reflected by the overcoupled resonator. We did not take any special measures beyond the receiver protection switch (Doll and Jeschke, 2017) . However, we are planning to install an additional limiter or a slow switch that could take more power. Since the spin-lock pulses are rather long, a slow switch could be used for most of the time , while the fast switch could be used for the transient times of the pulses to still provide the small dead time.

As model compounds, we used bis-trityl rulers with electron-electron distances of about 4.1 nm and 5.3 nm. The synthesis is discussed in section 4.1. The bis-trityl rulers were dissolved in *ortho*-terphenyl (OTP) or its perdeuterated analogue dOTP providing solutions of different concentrations. More details are given in each figure and the SI.

Measurements were conducted at 50 K using a liquid helium flow cryostat. We did not systematically test the optimal temperature for each measurement. However, it is likely that higher temperatures would allow for shorter shot repetition times without dramatically changing the dephasing times.

Frequency-domain spectra were measured with chirp echoes and subsequent Fourier transform instead of field sweeps (Doll and Jeschke, 2014). Chirp pulses covered a range of 300 MHz symmetrically around the centre of the spectrum. The powder spectrum was simulated with the *EasySpin* library (Stoll and Schweiger, 2006).

The two-pulse dephasing time T_m was measured with a sequence $\pi/2-\tau-\pi-\tau-$ echo with $t_\pi = 2t_\pi$. Different pulse lengths were used to check whether instantaneous diffusion contributes to coherence loss. Similar to previous findings by Meyer et al. (2018), it was found that flip angles of $\pi/2$ or $3\pi/2$ for the second pulse gave higher echo intensities than an angle of π. More details are given in the SI.

The rotating frame relaxation time $T_{1\rho}$ was measured with the sequence in Fig. 1 in the absence of any phase-modulation pulses and variable T_{SL} and with τ_{SL} =200 ns. Interestingly, $T_{1\rho}$ is significantly different when measured with a simple spin-locked echo with the sequence $\pi/2-\tau-$ lock $-\tau-$ echo. More details are given in the results section and the SI.

The rotating frame relaxation time $T_{2\rho}$ for the mono-trityl was measured with the sequence in Fig. 1 including the phase-modulation pulses and fixed T_{SL} and with τ_{SL} =200 ns. In the case of the bis-trityls, it is impossible to measure $T_{2\rho}$ independent of the dipolar coupling. Where applicable, we mention the decay rate of the "intramolecular background" for comparison.

All decay rates were obtained by fitting a stretched exponential of the functional form

$$f(t) = \exp\left(-(t/T)^{\xi/3}\right) \tag{19}$$

to the relaxation curves, where $t = 2\tau$ and $T = T_m$ for the two-pulse echo decay, $t = 2\tau_1$ and $T = T_{2\rho}$ for dressed echo decays, and $t = T_{\text{SL}}$ and $T = T_{1\rho}$ for the longitudinal rotating frame relaxation time.

The Rabi frequency ω_1 was measured with a nutation experiment $t_{\text{nut}} - T - \pi/2 - \tau - \pi - \tau -$ echo. As a control, we performed a dressed-spin resonance experiment with the sequence in Fig. (4), but only one PM pulse with low amplitude and variable frequency. This also yields the ω_1 spectrum (see the SI). A similar experiment with z-modulation was demonstrated in (Jeschke, 1999).

When the Rabi spectrum is known, one can set the value of the PM frequency ω_{PM}. One then needs to choose a value for the modulation amplitude a_{PM} and set up the PM pulse lengths. This can be achieved with a PM nutation experiment. Again, one uses the basic sequence in Fig. 1, with one pulse only with now fixed ω_{PM}. One then observes the echo intensity as a function of the PM pulse length. That way the optimal PM pulse length can be determined. When choosing $a_{\text{PM}} = 0.3$, we observed only slight Bloch-Siegert shift related oscillations in the PM pulse nutation traces while achieving a PM π-pulse length of 40-42 ns.

The dressed echo can not be detected directly, because τ_1 and τ_2 are both indirect variables. Only the actual echo at the end of the microwave pulse sequence is digitized continuously. In order to optimize indirect detection, we checked that the last PM pulse in Fig. 1 is applied at the correct position. We observed that the position seems to be nearly perfectly predictable by setting $\tau_2 = \tau_1 + t_{\pi/2}$, where $t_{\pi/2}$ refers to the length of the PM-$\pi/2$-pulse. We observed crossing dressed-spin echoes when changing interpulse delays in the PM pulse sequence, similar to what is known in microwave multi-pulse sequences in pulse EPR. Interestingly, the position of some unwanted echoes depends on the choice of τ_0. Nevertheless, all these unwanted echoes can be suppressed by phase cycling the initial phases ϕ_{PM} of the PM pulses, ϕ_{2-4}.

A step-by-step guide to setting up the sequence is provided in the SI.

4 Results

4.1 Synthesis

The synthesis of bis-trityl rulers **1** and **2** is presented in Fig. 2. They were assembled from the rodlike building blocks **6** equipped with amino groups at both ends and trityl acid chloride **8**. The latter was prepared from the corresponding trityl acid **7** (also named mono-trityl) using a procedure that has been described for the corresponding conversion of the structurally related Finland trityl radical (Shevelev et al., 2014). To achieve a complete conversion of the building blocks **6**, trityl acid chloride **8** was used in excess. Leftover trityl acid chloride **8** is hydrolysed upon workup and the resulting trityl acid **7** is easily removed by filtration through silica gel. The building blocks **6** were obtained through a sequence of alkynyl-aryl coupling reactions (Sahoo et al., 2010; Qi et al., 2016; Ritsch et al., 2019) and a final oxidative alkyne dimerization. Oxidative alkyne dimerization is a very efficient way to obtain rod-like spacers with the same functional groups at both ends. Although this gives a butadiyne moiety, the spacer is still rather stiff and therefore the spin-spin distance sufficiently well-defined (Godt et al., 2006; Jeschke et al., 2010).

4.2 Relaxation of mono-trityl 7

As a reference, we measured the spectrum and the relaxation properties of the mono-trityl **7** in dOTP, see Fig. 3. As visible in panel (b), $T_{1\rho}$ is orders of magnitude larger than T_m. Unfortunately, our TWT prevents us from using spin-lock pulses of more than 40 µs, meaning that uncertainty in $T_{1\rho}$ is rather large. Nevertheless, fitting a single stretched exponential to each curve yields values of T_m =2.9 µs and $T_{1\rho}$ ≈930 µs. As mentioned above, the distance measurements based on dressed spin echoes are limited by the transverse rotating frame relaxation time $T_{2\rho}$ rather than the longitudinal one $T_{1\rho}$. The blue curve in panel (b) shows the dressed echo decay, indicating that $T_m < T_{2\rho} \ll T_{1\rho}$, with a fitted value of $T_{2\rho}$ =13.1 µs.

While conceptually simple, the large difference between $T_{1\rho}$ and $T_{2\rho}$ was rather surprising to us. We are not aware of any example in the literature where $T_{2\rho}$ is discussed in-depth in the context of EPR, although there are several discussion in NMR and MRI (Michaeli et al., 2004). It remains unclear what the limiting contribution to $T_{2\rho}$ is. In analogy to solid-state NMR, residual coupling terms of the hyperfine interactions certainly contribute. An additional contribution would be the remaining intermolecular dipolar couplings, but then we would expect a strong dependence on the concentration, which we did not observe. Another factor that will definitely contribute is the noise of the driving field (Cohen et al., 2017). The noise (phase and amplitude) of the TWT during spin-lock will not be refocused by the dressed echo. It is hard to quantify this contribution, since we do not have high-power amplifiers with different noise figures. In the future, we might investigate the influence of artificially added driving noise on $T_{2\rho}$.

The large difference between $T_{1\rho}$ and $T_{2\rho}$ is unfortunate, because our proposed sequence will be limited by the latter. Nevertheless, one might come up with a sequence that will be limited by the former, longer relaxation time, and thus we measured $T_{1\rho}$ also for the bis-trityl rulers.

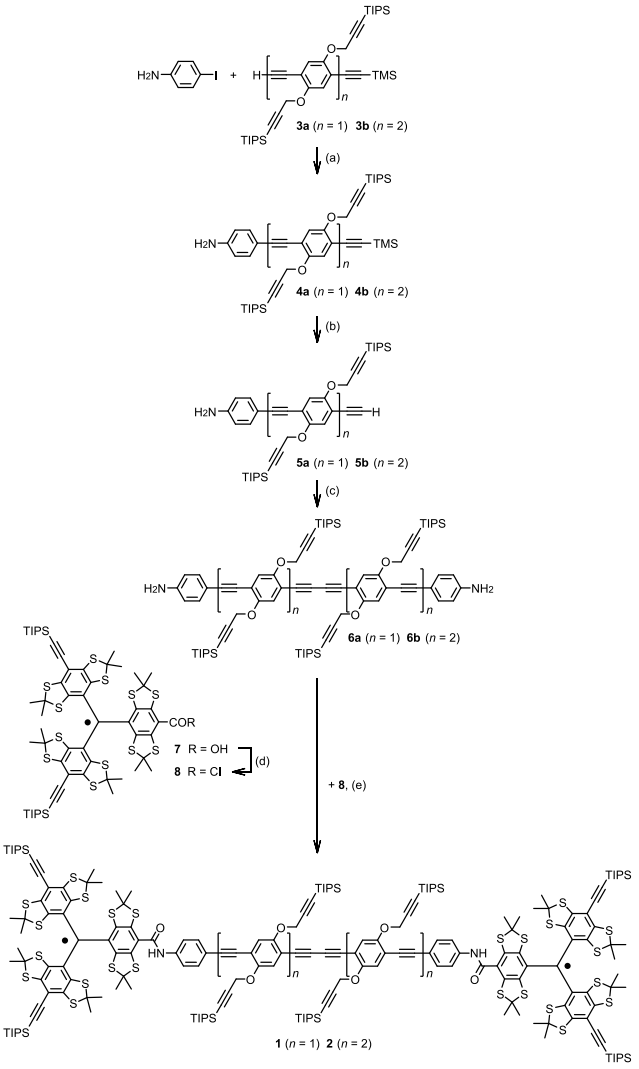

Figure 2. Synthesis of the bis-trityl rulers **1** and **2**. For n = 1: (a) $PdCl_2(PPh_3)_2$, CuI, piperidine, THF, rt, 25 h, 84%; (Ritsch et al., 2019) (b) K_2CO_3, MeOH, CH_2Cl_2, rt, 14.5 h, 96%; (c) $PdCl_2(PPh_3)_2$, CuI, piperidine, THF, air, rt, 16 h, 36%; (d) $SOCl_2$, $CHCl_3$, 50 °C, 90 min, not isolated; (e) $^{i}Pr_2NEt$, $CHCl_3$, rt, 17 h, 40%. For n = 2: (a) $PdCl_2(PPh_3)_2$, CuI, piperidine, THF, rt, 46 h, 86%; (b) K_2CO_3, MeOH, CH_2Cl_2, rt, 14.5 h, 96%; (c) $PdCl_2(PPh_3)_2$, CuI, piperidine, THF, air, rt, 15.5 h, 65%; (d) $SOCl_2$, $CHCl_3$, 50 °C, 90 min, not isolated; (e) $^{i}Pr_2NEt$, $CHCl_3$, rt, 19 h, 64%. For further details see the SI part B. THF = tetrahydrofuran, TIPS = triisopropylsilyl, TMS = trimethylsilyl, rt = room temperature.

4.3 Bis-trityl 1, $r \approx 4.1$ nm

The results for bis-trityl **1** are shown in Fig. 4. The chirp echo FT-EPR spectrum is shown in panel (a). The spectrum consists of a slightly asymmetric line with an FWHM of 16 MHz. The theoretical excitation profile of a 4 ns and an 8 ns microwave pulse are overlaid, showing that the whole spectrum can be excited almost uniformly with rectangular pulses.

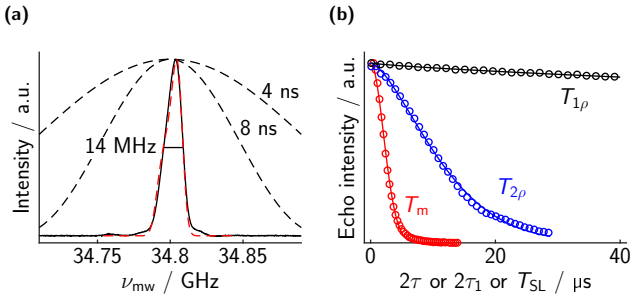

Figure 3. Measurements on mono-trityl **7**. (**a**) EPR spectrum. The excitation profiles of the rectangular pulses used are indicated. They are sufficiently strong to excite the whole EPR line. The red dashed lines indicate a simulation based on the g-values given in (Hintz et al., 2019) and an Gaussian broadening of 8 MHz FWHM. (**b**) Corresponding echo decay curves. Experimental points in circles (not all points shown for clarity), and best fit in solid lines. The fitted values are T_m =2.9 µs ($\xi = 5.9$), $T_{2\rho}$ =13.1 µs ($\xi = 4.6$) and $T_{1\rho}$ =930 µs ($\xi = 2.4$).

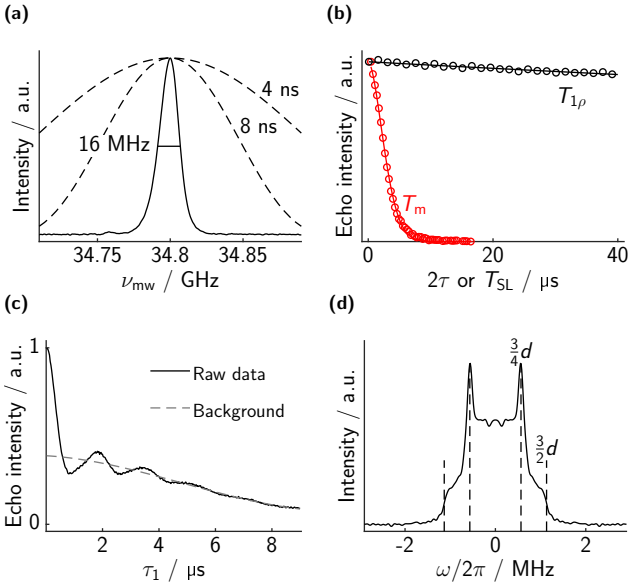

Figure 4. Measurements on bis-trityl **1**. (**a**) EPR spectrum. (**b**) Comparison of the decay of a microwave two-pulse echo (red, bare-spin decoherence) with the decay of the spin-locked echo as a function of T_{SL} (black, dressed-spin polarization decay). Experimental points in circles (not all points shown for clarity), and best fit in solid lines. The fitted values are T_m =3.3 µs ($\xi = 5.3$), and $T_{1\rho}$ =560 µs ($\xi = 2.9$) (**c**) Dressed-spin echo evolution as a function of $\tau_1 = \tau_2$. The dipolar oscillations are clearly visible. A stretched exponential background with $T_{2\rho}$ =14.3 µs ($\xi = 5.4$) is shown in gray. (**d**) Dipolar spectrum obtained by a Fourier transform of (**c**) after background division. The positions of the expected singularities based on the distance of the electrons are indicated by dashed lines. Note that there are small artifact peaks outside the plotting range at ±8 MHz which we suspect to be a sampling artifact.

The relaxation measurements for T_m and $T_{1\rho}$ are displayed in panel (b), and they show the same trends as in the case of the mono-trityl. Note that the T_m measurement displayed was done with 100/200 ns pulses. Otherwise, the dipolar oscillations are already strongly visible in the two-pulse echo decay. It is immediately clear that the rotating frame relaxation time $T_{1\rho}$ is much longer than the phase-memory time, $T_{1\rho} \gg T_{\mathrm{m}}$. The phase memory time is about 3.3 µs, while after 40 µs of spin-lock, the echo intensity is still more than 90 % of its maximal value. A naive fit with a stretched exponential yields $T_{1\rho} \approx 560$ µs.

The modulation of the dressed-spin echo is displayed in panel (c). Clear oscillations are visible in the primary data. Since we do not currently have a model for the background, we fitted a stretched exponential to the data. This background is very similar to the $T_{2\rho}$ measurement of the mono-trityl (14.3 µs *vs.* 13.1 µs decay constant), which also means that it decays much faster than $T_{1\rho}$. Note that not only intermolecular dipolar couplings from remote spins contribute to the background. Transverse relaxation of dressed spins with time constant $T_{2\rho}$ also contributes because we do not perform a constant time experiment. Regarding modulation depth we would have expected it to be unity, which is clearly not seen in our experiments. We suspect that imperfections in the dressed spin π -pulse lead to an unmodulated background, which cannot be removed by phase-cycling. The phenomenon is similar to reduced instantaneous diffusion for a Hahn echo if the flip angle of the π -pulse is reduced.

After background correction by division and a Fourier transform, we obtain the spectrum in Fig. 4 (d). The spectrum is a nice Pake pattern with the characteristic singularities at one and two times the dressed-spin dipolar frequency. The singularities appear at the expected positions. The splitting parameter d can be calculated from the expected distance of 4.1 nm, but it is scaled by a factor of $3/4$ as discussed above.

4.4 Bis-trityl 2, $r \approx 5.3$ nm

The analogous data of bis-trityl **2** are displayed separately in Fig. 5. The chirp echo FT EPR spectrum looks essentially the same as for bis-trityl **1**, with the same slight asymmetry and an FWHM of 16 MHz.

The two-pulse microwave echo decay is slightly faster for bis-trityl **2** (2.9 µs vs. 3.3 µs). Again, it is difficult to really quantify a decoherence time that is not influenced by residual echo envelope contributions from intramolecular electron-electron coupling. Even with 100/200 ns pulses the excitation profile of the π-pulse is still larger than the dipolar coupling and some dipolar contribution to the echo envelope function is expected. The signal decay of dressed spin polarization under the spin-lock ($T_{1\rho} = 730$ µs) is again much slower, and comparable to the case of bis-trityl **1**. Unfortunately, the dipolar oscillations in panel (c) are not as clear as in the case of shorter distances. Also, the background is already rather fast compared to the dipolar frequencies (14.5 µs decay constant). In the dipolar spectrum, panel (d), it becomes clear that this case is more complicated, because additional singularities appear at around $3/8 \cdot d$. These features must result from the breakdown of some approximation that we have made in our theoretical description. Most likely they are due to the finite strength of the spin-lock compared to the inhomogeneous spectral width. For two spins with different bare-spin resonance offsets, both the direction and magnitude of the effective field in the rotating frame differs. Accordingly, the two dressed spins have different resonance frequencies and quantization axes. Unless the dipole-dipole coupling is much larger than the frequency difference, it is significantly perturbed. In order to give a more quantitative explanation, we will show simplified numerical simulations in the following.

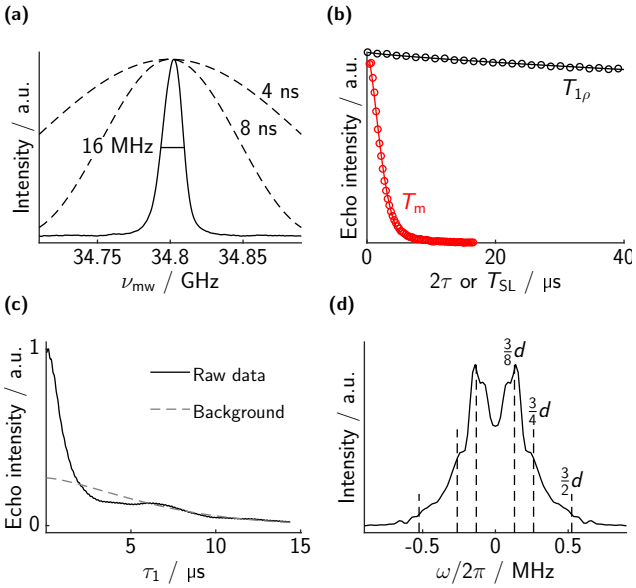

Figure 5. (Measurements on bis-trityl **2**. **a**) EPR spectrum. (**b**) Bare-spin decoherence (two-pulse echo decay, red) and dressed-spin polarization decay (spin-locked echo decay, black). Experimental points in circles (not all points shown for clarity), and best fit in solid lines. The fitted values are T_m =2.6 µs ($\xi = 4.9$), and $T_{1\rho}$ ≈730 µs ($\xi = 2.4$) (**c**) PM echo evolution as a function of $\tau_1 = \tau_2$. A stretched exponential background with $T_{2\rho}$ =14.5 µs ($\xi = 4.4$) is shown in gray. The dipolar oscillations are damped and the background obscures the oscillations at long dipolar evolution times. (**d**) Dipolar spectrum obtained by a Fourier transform of (**c**) after background division. In addition to the singularities expected from our basic theoretical treatment strong singularities at $3/8d$ are apparent. These features are explained in the main text.

4.5 Numerical Simulations

In order to understand the deviation of our experimental results from the theoretical expectation based on first-order average Hamiltonian theory (especially in the case of bis-trityl **2**), we performed simplified numerical simulations. In principle, one could simulate the complete sequence, including the time-dependent phase during the phase-pulses. We chose a simplified route: We start with both spins along z' and then calculate the expectation value of $\hat{S}_z = \hat{S}_{1z} + \hat{S}_{2z}$ during the spin lock using the Hamiltonian

$$\begin{aligned}\hat{\mathcal{H}}' =& \Omega_1 \hat{S}_{1z} + \Omega_2 \hat{S}_{2z} \\ &+ \omega_{\mathrm{dd}}(r,\theta)\left(\hat{S}_{1z}\hat{S}_{2z} - \frac{1}{2}\left(\hat{S}_{1x}\hat{S}_{2x} + \hat{S}_{1y}\hat{S}_{2y}\right)\right) \\ &+ 2\pi \cdot \nu_1(t)\left(\hat{S}_{1x} + \hat{S}_{2x}\right)\end{aligned} \tag{20}$$

In order to refocus the nutation of the spins around the effective field, we invert the phase of the irradiation in the middle of the spin-lock, such that

$$\nu_1(t) = \begin{cases} \nu_1(0), & \text{for } 0 \leq t < \tau_1 \\ -\nu_1(0), & \text{for } \tau_1 \leq t < 2\tau_1 \end{cases} . \tag{21}$$

This emulates the effect of the dressed refocusing (phase) pulse. With this choice, the evolution consists of two periods with time-independent Hamiltonians, which is straight-forward to calculate on a computer.

In our implementation, which is available online, the parameters Ω_1, Ω_2, r, and θ are drawn in Monte-Carlo fashion from their respective distributions (Gaussian for the first three, $P(\theta) = \sin(\theta)$ with $0 \leq \theta \leq \pi/2$ for the latter). Statistical independence of the parameters is assumed. It is not unlikely that this assumption is at least partially wrong, since the respective orientation of the trityl moieties is restricted by the rigid linker. Although we have implemented simulations with a distance distribution, we do not consider such cases here but rather assume fixed values of r. Additionally, all the simulations shown here assume on-resonance irradiation in the sense that the mean values of Ω_1 and Ω_2 are 0.

Some illustrative simulations are shown in Fig. 6. For each parameter set, we display the numerical simulation in time and frequency domain as solid lines and show the analytical dipolar powder pattern (scaled by 3/4) as dashed lines on top. In panel (a), we show simulations assuming infinitely narrow EPR lines. In this case, the numerical and analytical results are the same. Panel (b) shows a simulation were we assume a FWHM of 16 MHz for both offset distributions (denoted by Γ_Ω). For the case of $r = 5.3$ nm, the simulation qualitatively reproduces the experimental results for bis-trityl **2**, especially regarding the singularities in the dipolar spectra. For $r = 4.1$ nm, the experimental results actually look better than the simulation if one regards the additional singularities at $3/8 \cdot d$ as an artifact. In this case, simulations with $\Gamma_\Omega = 8$ MHz are actually closer to the experimental results (see panel (c)). This might suggest that the difference in offsets of bis-trityl **1** is smaller than the EPR spectrum might suggest. Either hyperfine and dipolar couplings significantly contribute to the linewidth of the EPR spectrum, or the offsets are not completely uncorrelated in reality. In order to guide future developments, we also simulated traces assuming $\Gamma_\Omega = 8$, but with significantly larger microwave strengths of ν_1=200/400 MHz, see panel (d). Compared to panels (b) and (c), these simulations already show much better defined dipolar spectra. In conclusion, the simulations confirm that at least some of the artifacts in the experimental results are due to the finite size of the electron spin nutation frequency. The contribution of the artifacts becomes larger for larger offset differences and smaller dipolar couplings.

5 Conclusions and outlook

We showed that it is possible to measure the dipolar coupling between trityl radicals during a spin-lock by using short intervals of phase-modulations, *i.e.* by a *dressed*-spin echo generated with PM pulses. The relaxation during the spin lock is much slower compared to a simple two-pulse echo decay. The phenomena can be conceptually understood by describing the spin-lock in a nutating frame and using average Hamiltonian theory. For an electron-electron distance of ≈4.1 nm, the experimental spectra agree very well with the theoretical expectations that assume a microwave Rabi frequency much larger than all other interac-

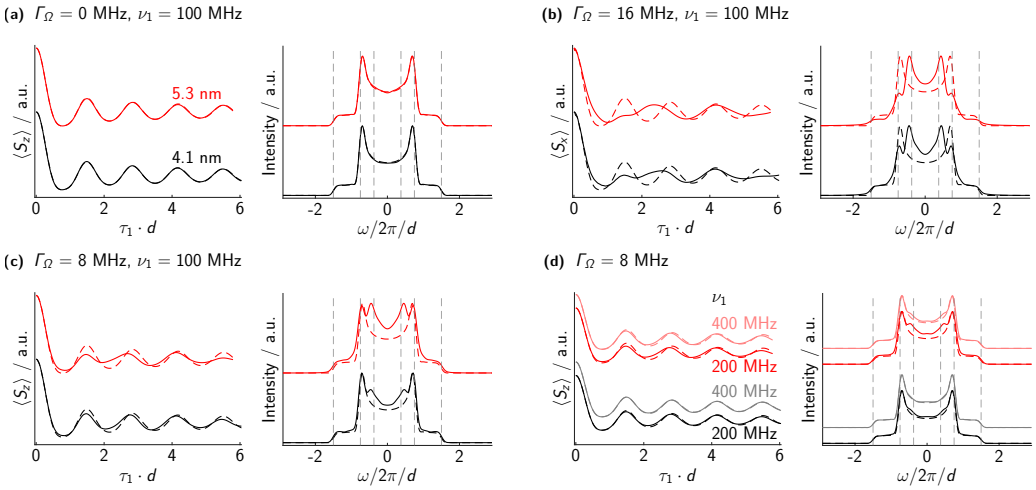

Figure 6. Numerical simulations with different dipolar couplings, offset distributions, and Rabi frequencies. Time and frequency axes are scaled by the dipolar coupling to facilitate comparison. Dashed lines represent the analytical Pake pattern (with the frequency scaled by 3/4). **(a)** No offsets at all, 100 MHz Rabi frequency. The numerical simulation of the spin-lock completely matches the analytical expectation. **(b)** Gaussian offset distribution with FWHM of 16 MHz, 100 MHz Rabi frequency. The numerical simulations deviate from the analytical expectation. In the frequency domain, "artifacts" appear at lower frequencies, around $3/8 \cdot \nu_\perp$. **(c)** Same as **(b)**, but with reduced offset FWHM of only 8 MHz. The intensity of the artifacts is reduced compared to larger offset distributions. **(d)** same as **(c)**, but with increased Rabi frequencies. The intensity of the artifacts is again reduced compared to smaller Rabi frequencies.

tions in the system. For a distance of ≈5.3 nm, additional singularities appear in the dipolar spectrum. While the spin dynamics underlying these additional contributions can be understood by numerical simulations, they might seriously complicate data analysis in terms of distance distributions and have to be addressed in the future, if the sequence should be used in application work. Additionally, we showed a profound difference between the longitudinal and transverse rotating frame relaxation times, $T_{1\rho}$ and $T_{2\rho}$. In our case, the latter is much smaller than the former and unfortunately limits the distance measurements by the sequence introduced here. Preliminary results with the OX063 trityl and its partially deuterated analogue OX71 in different solvent compositions (not shown) revealed that even bare-spin relaxation at low temperatures and low concentrations is complicated to understand, let alone dressed-spin relaxation with characteristic times $T_{2\rho}$ and $T_{1\rho}$. We are planning to investigate this in more detail. Note that in dOTP, the T_m values of the slow relaxing component of nitroxides (the relaxation of nitroxides in dOTP can be described by a sum of two stretched exponentials) can still be bigger than the $T_{2\rho}$ times measured here for trityl radicals (Soetbeer et al., 2018).

Since there are still significant artifacts present in the dipolar spectra when measuring longer distances, we refrained from a systematic analysis of signal-to-noise ratio and a comparison with existing pulse sequences.

Nevertheless, we are confident that the presented obstacles can be overcome. First, it might very well be possible to come up with a dressed pulse sequence that measures the dipolar coupling with an observation time limited by $T_{1\rho}$ instead of $T_{2\rho}$. This

appears feasible because, unlike the sum of dressed spin polarizations of the two spins, their difference is affected by dipolar coupling. This fact is used in cross-polarization in solid-state NMR and oscillatory behavior of magnetization transfer in the rotating frame has been studied in the context of heteronuclear correlation spectroscopy (Müller and Ernst, 1979). Second, the ratio of Rabi frequency to offsets could be reduced by going to a lower field. While in principle we could have done the experiments at X-band frequencies, our TWT in this range can only generate pulses of up tp 15 µs. The Rabi frequencies generated by our setup are already rather high ($\approx$ 100 MHz compared to $\approx$50 MHz in most commercial setups), but several groups around the world are working on micro resonators (Anders and Lips, 2019; Sidabras et al., 2019; Narkowicz et al., 2008; Blank et al., 2017), which generally give higher conversion factors and could be used to generate higher Rabi frequencies. If these difficulties can be overcome, pulse dressed electron paramagnetic resonance could significantly expand the measurable distance range, at least for trityl radicals.

Code and data availability. Experimental data, processing scripts, and simulation scripts in MATLAB are available online. DOI: 10.5281/zenodo.3703053

Author contributions. NW designed the research with input from GJ. HH synthesized the bis-trityl rulers under the supervision of AG. NW carried out all measurements, data analysis and simulations with help from AV. The EPR part of the manuscript was written by NW and edited by GJ and AG. The synthetic part was written by HH and AG.

Competing interests. The authors declare that they have no con-flict of interest.

Acknowledgements. This work was financed by ETH Zürich (grant ETH-48 16-1) and the Deutsche Forschungsgemeinschaft within SPP 1601 (GO 555/6-2). We thank Lukas Schreder, who carried out a research project in a very independent manner and sparked NW's interest in dressed electron spin resonance. We thank Jan Henrik Ardankjær-Larsen for providing OX063 and OX071 for preliminary relaxation studies. Matthias Ernst is acknowledged for helpful discussions and critically reading the theoretical part of the article.

References

Anders, J. and Lips, K.: MR to go, Journal of Magnetic Resonance, 306, 118–123, https://doi.org/10.1016/j.jmr.2019.07.007, 2019.

Blank, A.: A new approach to distance measurements between two spin labels in the >10 nm range, Physical Chemistry Chemical Physics, 19, 5222–5229, https://doi.org/10.1039/C6CP07597E, 2017.

Blank, A., Twig, Y., and Ishay, Y.: Recent trends in high spin sensitivity magnetic resonance, Journal of Magnetic Resonance, 280, 20–29, https://doi.org/10.1016/j.jmr.2017.02.019, 2017.

Borbat, P. P. and Freed, J. H.: Multiple-quantum ESR and distance measurements, Chemical Physics Letters, 313, 145–154, https://doi.org/10.1016/S0009-2614(99)00972-0, 1999.

Borbat, P. P., Georgieva, E. R., and Freed, J. H.: Improved sensitivity for long-distance measurements in biomolecules: Five-pulse double electron-electron resonance, Journal of Physical Chemistry Letters, 4, 170–175, https://doi.org/10.1021/jz301788n, 2013.

Bordignon, E. and Bleicken, S.: New limits of sensitivity of site-directed spin labeling electron paramagnetic resonance for membrane proteins, Biochimica et Biophysica Acta - Biomembranes, 1860, 841–853, https://doi.org/10.1016/j.bbamem.2017.12.009, 2018.

Breitgoff, F. D., Soetbeer, J., Doll, A., Jeschke, G., and Polyhach, Y. O.: Artefact suppression in 5-pulse double electron electron resonance for distance distribution measurements, Physical Chemistry Chemical Physics, 19, 15 766–15 779, https://doi.org/10.1039/C7CP01488K, 2017.

Brown, I. M.: Electron spin-echo studies of relaxation processes in molecular solids, in: Time Domain Electron Spin Resonance, edited by Kevan, L. and Schwartz, R., p. 200, John Wiley and Sons, Inc, New York, 1979.

Chen, H.-Y. and Tycko, R.: Slice Selection in Low-Temperature, DNP-Enhanced Magnetic Resonance Imaging by Lee-Goldburg Spin-Locking and Phase Modulation, Journal of Magnetic Resonance, p. 106715, https://doi.org/https://doi.org/10.1016/j.jmr.2020.106715, 2020.

Cohen, I., Aharon, N., and Retzker, A.: Continuous dynamical decoupling utilizing time-dependent detuning, Fortschritte der Physik, 65, 1–7, https://doi.org/10.1002/prop.201600071, 2017.

Cohen-Tannoudji, C., Dupont-Roc, J., and Grynberg, G.: Atom-Photon Interactions, 1992.

Doll, A.: Frequency-Swept Microwave Pulses for Electron Spin Resonance, Ph.D. thesis, ETH Zurich, https://doi.org/http://dx.doi.org/10.3929/ethz-a-010670425, 2016.

Doll, A. and Jeschke, G.: Fourier-transform electron spin resonance with bandwidth-compensated chirp pulses, Journal of Magnetic Resonance, 246, 18–26, https://doi.org/10.1016/j.jmr.2014.06.016, 2014.

Doll, A. and Jeschke, G.: Wideband frequency-swept excitation in pulsed EPR spectroscopy, Journal of Magnetic Resonance, 280, 46 – 62, https://doi.org/https://doi.org/10.1016/j.jmr.2017.01.004, special Issue on Methodological advances in EPR spectroscopy and imaging, 2017.

Duss, O., Yulikov, M., Jeschke, G., and Allain, F. H.-T.: EPR-aided approach for solution structure determination of large RNAs or protein-RNA complexes., Nature communications, 5, 3669, https://doi.org/10.1038/ncomms4669, 2014.

Ernst, M.: Heteronuclear spin decoupling in solid-state NMR under magic-angle sample spinning, vol. 162, https://doi.org/10.1016/S1090-7807(03)00074-0, 2003.

Georgieva, E. R., Ramlall, T. F., Borbat, P. P., Freed, J. H., and Eliezer, D.: The Lipid-binding Domain of Wild Type and Mutant a-Synuclein, Journal of Biological Chemistry, 285, 28 261–28 274, https://doi.org/10.1074/jbc.m110.157214, 2010.

Godt, A., Schulte, M., Zimmermann, H., and Jeschke, G.: How Flexible Are Poly(para-phenyleneethynylene)s?, Angewandte Chemie International Edition, 45, 7560–7564, https://doi.org/10.1002/anie.200602807, 2006.

Grzesiek, S. and Bax, A.: Audio-Frequency NMR in a Nutating Frame. Application to the Assignment of Phenylalanine Residues in Isotopically Enriched Proteins, Journal of the American Chemical Society, 117, 6527–6531, https://doi.org/10.1021/ja00129a016, 1995.

Hintz, H., Vanas, A., Klose, D., Jeschke, G., and Godt, A.: Trityl Radicals with a Combination of the Orthogonal Functional Groups Ethyne and Carboxyl: Synthesis without a Statistical Step and EPR Characterization, The Journal of Organic Chemistry, 84, 3304–3320, https://doi.org/10.1021/acs.joc.8b03234, https://doi.org/10.1021/acs.joc.8b03234, pMID: 30785294, 2019.

Hoult, D. I.: Rotating frame zeugmatography, Journal of Magnetic Resonance (1969), 33, 183–197, https://doi.org/10.1016/0022-2364(79)90202-6, 1979.

Jeschke, G.: Coherent superposition of dressed spin states and pulse dressed electron spin resonance, Chemical Physics Letters, 301, 524–530, https://doi.org/10.1016/S0009-2614(99)00041-X, 1999.

Jeschke, G.: DEER Distance Measurements on Proteins., Annual review of physical chemistry, 63, 419–46, https://doi.org/10.1146/annurev-physchem-032511-143716, 2012.

Jeschke, G. and Schweiger, A.: Hyperfine decoupling in electron spin resonance, Journal of Chemical Physics, 106, 9979–9991, https://doi.org/10.1063/1.474073, 1997.

Jeschke, G., Pannier, M., Godt, A., and Spiess, H.: Dipolar spectroscopy and spin alignment in electron paramagnetic resonance, Chemical Physics Letters, 331, 243–252, https://doi.org/10.1016/S0009-2614(00)01171-4, 2000.

Jeschke, G., Sajid, M., Schulte, M., Ramezanian, N., Volkov, A., Zimmermann, H., and Godt, A.: Flexibility of shape-persistent molecular building blocks composed of p-phenylene and ethynylene units, Journal of the American Chemical Society, 132, 10 107–10 117, https://doi.org/10.1021/ja102983b, 2010.

Klauder, J. R. and Anderson, P. W.: Spectral Diffusion Decay in Spin Resonance Experiments, Physical Review, 125, 912–932, https://doi.org/10.1103/PhysRev.125.912, 1962.

Kulik, L. V., Dzuba, S. A., Grigoryev, I. A., and Tsvetkov, Y. D.: Electron dipole-dipole interaction in ESEEM of nitroxide biradicals, Chemical Physics Letters, 343, 315–324, https://doi.org/10.1016/S0009-2614(01)00721-7, 2001.

Laucht, A., Simmons, S., Kalra, R., Tosi, G., Dehollain, J. P., Muhonen, J. T., Freer, S., Hudson, F. E., Itoh, K. M., Jamieson, D. N., McCallum, J. C., Dzurak, A. S., and Morello, A.: Breaking the rotating wave approximation for a strongly driven dressed single-electron spin, Physical Review B, 94, 1–5, https://doi.org/10.1103/PhysRevB.94.161302, 2016.

Laucht, A., Kalra, R., Simmons, S., Dehollain, J. P., Muhonen, J. T., Mohiyaddin, F. A., Freer, S., Hudson, F. E., Itoh, K. M., Jamieson, D. N., McCallum, J. C., Dzurak, A. S., and Morello, A.: A dressed spin qubit in silicon, Nature Nanotechnology, 12, 61–66, https://doi.org/10.1038/nnano.2016.178, 2017.

Meyer, A., Jassoy, J. J., Spicher, S., Berndhäuser, A., and Schiemann, O.: Performance of PELDOR, RIDME, SIFTER, and DQC in measuring distances in trityl based bi- and triradicals: Exchange coupling, pseudosecular coupling and multi-spin effects, Physical Chemistry Chemical Physics, 20, 13 858–13 869, https://doi.org/10.1039/c8cp01276h, 2018.

Michaeli, S., Sorce, D. J., Idiyatullin, D., Ugurbil, K., and Garwood, M.: Transverse relaxation in the rotating frame induced by chemical exchange, Journal of Magnetic Resonance, 169, 293 – 299, https://doi.org/https://doi.org/10.1016/j.jmr.2004.05.010, 2004.

Milikisyants, S., Scarpelli, F., Finiguerra, M. G., Ubbink, M., and Huber, M.: A pulsed EPR method to determine distances between paramagnetic centers with strong spectral anisotropy and radicals: The dead-time free RIDME sequence, Journal of Magnetic Resonance, 201, 48–56, https://doi.org/10.1016/j.jmr.2009.08.008, 2009.

Milov, A. D., Ponomarev, A. B., and Tsvetkov, Y. D.: Electron-electron double resonance in electron spin echo: Model biradical systems and the sensitized photolysis of decalin, Chemical Physics Letters, 110, 67–72, https://doi.org/10.1016/0009-2614(84)80148-7, 1984.

Müller, L. and Ernst, R.: Coherence transfer in the rotating frame, Molecular Physics, 38, 963–992, https://doi.org/10.1080/00268977900102161, 1979.

Narkowicz, R., Suter, D., and Niemeyer, I.: Scaling of sensitivity and efficiency in planar microresonators for electron spin resonance, Review of Scientific Instruments, 79, https://doi.org/10.1063/1.2964926, 2008.

Pannier, M., Veit, S., Godt, A., Jeschke, G., and Spiess, H. W.: Dead-Time Free Measurement of Dipole-Dipole Interactions between Electron Spins, Journal of Magnetic Resonance, 142, 331–340, https://doi.org/10.1006/jmre.1999.1944, 2000.

Qi, M., Hülsmann, M., and Godt, A.: Spacers for Geometrically Well-Defined Water-Soluble Molecular Rulers and Their Application, Journal of Organic Chemistry, 81, 2549–2571, https://doi.org/10.1021/acs.joc.6b00125, 2016.

Redfield, A. G.: Nuclear magnetic resonance saturation and rotary saturation in solids, Physical Review, 98, 1787–1809, https://doi.org/10.1103/PhysRev.98.1787, 1955.

Reginsson, G. W., Kunjir, N. C., Sigurdsson, S. T., and Schiemann, O.: Trityl radicals: Spin labels for nanometer-distance measurements, Chemistry - A European Journal, 18, 13 580–13 584, https://doi.org/10.1002/chem.201203014, 2012.

Rhim, W.-K., Pines, A., and Waugh, J. S.: Violation of the Spin-Temperature Hypothesis, Physical Review Letters, 25, 218–220, https://doi.org/10.1103/PhysRevLett.25.218, 1970.

Ritsch, I., Hintz, H., Jeschke, G., Godt, A., and Yulikov, M.: Improving the Accuracy of Cu(II)-Nitroxide RIDME in the Presence of Orientation Correlation Evaluated with Water-soluble Cu(II)-Nitroxide Rulers, Physical Chemistry Chemical Physics, https://doi.org/10.1039/C8CP06573J, 2019.

Sahoo, D., Thiele, S., Schulte, M., Ramezanian, N., and Godt, A.: Polar tagging in the synthesis of monodisperse oligo(p-phenyleneethynylene) s and an update on the synthesis of oligoPPEs, Beilstein Journal of Organic Chemistry, 6, 20–24, https://doi.org/10.3762/bjoc.6.57, 2010.

Saiko, A. P., Fedaruk, R., and Markevich, S. A.: Suppression of electron spin decoherence in Rabi oscillations induced by an inhomogeneous microwave field, Journal of Magnetic Resonance, 290, 60–67, https://doi.org/10.1016/j.jmr.2018.02.003, 2018.

Schmidt, T., Wälti, M. A., Baber, J. L., Hustedt, E. J., and Clore, G. M.: Long Distance Measurements up to 160 Å in the GroEL Tetradecamer Using Q-Band DEER EPR Spectroscopy, Angewandte Chemie - International Edition, 55, 15 905–15 909, https://doi.org/10.1002/anie.201609617, 2016.

Shevelev, G. Y., Krumkacheva, O. A., Lomzov, A. A., Kuzhelev, A. A., Rogozhnikova, O. Y., Trukhin, D. V., Troitskaya, T. I., Tormyshev, V. M., Fedin, M. V., Pyshnyi, D. V., and Bagryanskaya, E. G.: Physiological-temperature distance measurement in nucleic acid using triarylmethyl-based spin labels and pulsed dipolar EPR spectroscopy, Journal of the American Chemical Society, 136, 9874–9877, https://doi.org/10.1021/ja505122n, 2014.

Sidabras, J. W., Duan, J., Winkler, M., Happe, T., Hussein, R., Zouni, A., Suter, D., Schnegg, A., Lubitz, W., and Reijerse, E. J.: Extending electron paramagnetic resonance to nanoliter volume protein single crystals using a self-resonant microhelix, Science Advances, 5, https://doi.org/10.1126/sciadv.aay1394, 2019.

Soetbeer, J., Hülsmann, M., Godt, A., Polyhach, Y., and Jeschke, G.: Dynamical decoupling of nitroxides in o-terphenyl: a study of temperature, deuteration and concentration effects, Phys. Chem. Chem. Phys., 20, 1615–1628, https://doi.org/10.1039/C7CP07074H, 2018.

Spindler, P. E., Waclawska, I., Endeward, B., Plackmeyer, J., Ziegler, C., and Prisner, T. F.: Carr-Purcell Pulsed Electron Double Resonance with Shaped Inversion Pulses, Journal of Physical Chemistry Letters, 6, 4331–4335, https://doi.org/10.1021/acs.jpclett.5b01933, 2015.

Stoll, S. and Schweiger, A.: EasySpin, a comprehensive software package for spectral simulation and analysis in EPR, Journal of Magnetic Resonance, 178, 42–55, https://doi.org/10.1016/j.jmr.2005.08.013, 2006.

Tschaggelar, R., Breitgoff, F. D., Oberhänsli, O., Qi, M., Godt, A., and Jeschke, G.: High-Bandwidth Q-Band EPR Resonators, Applied Magnetic Resonance, pp. 1–28, https://doi.org/10.1007/s00723-017-0956-z, 2017.

Ward, R., Bowman, A., Sozudogru, E., El-Mkami, H., Owen-Hughes, T., and Norman, D. G.: EPR distance measurements in deuterated proteins, Journal of Magnetic Resonance, 207, 164–167, https://doi.org/10.1016/j.jmr.2010.08.002, 2010.

Supporting Information - Part A
for
Distance measurement between trityl radicals by pulse dressed electron paramagnetic resonance with phase modulation

Nino Wili[1], Henrik Hintz[2], Agathe Vanas[1,‡], Adelheidt Godt[2], and Gunnar Jeschke[2]

[1] *Department of Chemistry and Applied Biosciences, Laboratory of Physical Chemistry, ETH Zurich, Vladimir-Prelog-Weg 2, 8093 Zurich, Switzerland. E-mail: gjeschke@ethz.ch, nwili@ethz.ch*

[1] *Faculty of Chemistry and Center for Molecular Materials (CM_2), Bielefeld University, Universitätsstrasse 25, 33615 Bielefeld, Germany*

Contents

S.1 Derivation of the nutating frame Hamiltonians

In this section we will show step-by-step how to derive the effective Hamiltonians in the nutating frame.

S.1.1 Interaction frame transformation

We can split a Hamiltonian $\hat{\mathcal{H}}$ arbitrarily into a dominant part $\hat{\mathcal{H}}_0$ and all the other terms, $\hat{\mathcal{H}}_1$.

$$\hat{\mathcal{H}} = \hat{\mathcal{H}}_0 + \hat{\mathcal{H}}_1 \quad . \tag{1}$$

We can then transform $\hat{\mathcal{H}}$ into an interaction frame with $\hat{\mathcal{H}}_0$ with the unitary transformation

$$\hat{U} = \hat{T} \exp\left(-i \int_0^t \hat{\mathcal{H}}_0(t_1) \mathrm{d}t_1 \right)$$

$$\hat{\mathcal{H}}' = \hat{U}^\dagger \hat{\mathcal{H}} \hat{U} \quad , \tag{2}$$

where $\hat{T}$ is the Dyson time-ordering operator and † indicates the transpose and complex conjugate. For a time-independent $\hat{\mathcal{H}}_0$, the expression simplifies to

$$\hat{U} = \exp\left(-i\hat{\mathcal{H}}_0 t\right) \quad . \tag{3}$$

The equation of motion of the density operator in the interaction frame is then given by

$$\frac{\mathrm{d}}{\mathrm{d}t}\rho' = -i\left[\hat{\mathcal{H}}' - \hat{\mathcal{H}}'_0, \rho'\right] \tag{4}$$

$$\hat{\mathcal{H}}' - \hat{\mathcal{H}}'_0 = \hat{\mathcal{H}}'_1 \tag{5}$$

i.e. the influence of $\hat{\mathcal{H}}_0$ is absorbed into the frame, and we only have to look at the non-dominant terms in the interaction frame. Most of these calculations only involve simple rotations in 3-dimensional space.

S.1.2 Rotating frame

For simplicity and illustration, we first look at an isolated spin-1/2 particle in a static magnetic field B_0 along the laboratory z-axis. If we irradiate this system with a linearly polarized electromagnetic field with frequency ω_{mw} and amplitude $2B_1$, the Hamiltonian in angular frequency units is given by

$$\hat{\mathcal{H}} = \omega_S \hat{S}_z + 2\omega_1 \cos\left(\omega_{\mathrm{mw}} t + \phi_{\mathrm{mw}}\right) \hat{S}_x \quad , \tag{6}$$

We now go into a rotating frame with frequency ω_{mw}. This corresponds to an interaction frame with $\omega_{\mathrm{mw}}\hat{S}_z$, *i.e.* $\hat{\mathcal{H}}_0 = \omega_{\mathrm{mw}}\hat{S}_z$, which leads to

$$\begin{aligned}\hat{\mathcal{H}}_1' =&\omega_S\hat{S}_z\\ &+2\omega_1\cos\left(\omega_{\mathrm{mw}}t+\phi_{\mathrm{mw}}\right)\left(\cos(\omega_{\mathrm{mw}}t)\hat{S}_x-\sin(\omega_{\mathrm{mw}}t)\hat{S}_y\right)\\ &-\omega_{\mathrm{mw}}\hat{S}_z\\ =&\Omega_S\hat{S}_z\\ &+\omega_1\left(\cos(\phi_{\mathrm{mw}})\hat{S}_x+\sin(\phi_{\mathrm{mw}})\hat{S}_y\right)\\ &+\omega_1\left(\cos(2\omega_{\mathrm{mw}}t+\phi_{\mathrm{mw}})\hat{S}_x-\sin(2\omega_{\mathrm{mw}}t+\phi_{\mathrm{mw}})\hat{S}_y\right) \quad ,\end{aligned} \tag{7}$$

where we used trigonometric identities and introduced the offset $\Omega_S = (\omega_S - \omega_{\mathrm{mw}})$. Equation (7) contains two rotating waves, one that rotates with ω_{mw} that is said to be *on-resonance*, and one that rotates with $-\omega_{\mathrm{mw}}$ and is thus far *off*-resonance. The rotating wave approximation (RWA) now simply neglects the counter-rotating component. More formally speaking, this corresponds to the first order average Hamiltonian, obtained by integrating over one modulation period, in this case $\tau_c = 2\pi/\omega_{\mathrm{mw}}$,

$$\bar{\hat{\mathcal{H}}}^{(1)} = \frac{1}{\tau_c}\int_0^{\tau_c}\hat{\mathcal{H}}(t_1)\mathrm{d}t_1 \quad . \tag{8}$$

Here, the bar indicates the average Hamiltonian, the number in parentheses indicates the order. Quite often, and also in the case of the RWA, this amounts to simply neglecting the remaining time-dependent terms, as they are off-resonant. For the Hamiltonian in Eq. (7) we obtain

$$\hat{\mathcal{H}}_1' \approx \Omega_S\hat{S}_z + \omega_1\left(\cos(\phi_{\mathrm{mw}})\hat{S}_x+\sin(\phi_{\mathrm{mw}})\hat{S}_y\right) \tag{9}$$

The second order contribution to the average Hamiltonian is given by

$$\bar{\hat{\mathcal{H}}}^{(2)} = \frac{-i}{2\tau_c}\int_0^{\tau_c}\int_0^{t_2}\left[\hat{\mathcal{H}}(t_2),\hat{\mathcal{H}}(t_1)\right]\mathrm{d}t_1\mathrm{d}t_2 \quad . \tag{10}$$

Evaluating the double-integral for Eq. (7) leads to the Bloch-Siegert shift Hamiltonian

$$\hat{\mathcal{H}}_{\mathrm{BS}} = \frac{1}{4}\frac{\omega_1^2}{\omega_{\mathrm{mw}}}\hat{S}_z \quad . \tag{11}$$

S.1.3 Nutating Frame

The truncated rotating frame Hamiltonian in Eq. (9) can be further simplified by assuming $\phi_{\mathrm{mw}} = 0$, which leaves us with

$$\hat{\mathcal{H}}' = \Omega_S\hat{S}_z + \omega_1\hat{S}_x \tag{12}$$

If the Rabi frequency is much larger than the resonance offset, $\omega_1 \gg \Omega_S$, the situation can be discussed by using another interaction frame transformation with $\omega_1 \hat{S}_x$. This term is then absorbed into the frame, and the rest transforms to

$$\hat{\mathcal{H}}'' = \Omega_S \left(\cos(\omega_1 t)\hat{S}_z + \sin(\omega_1 t)\hat{S}_y\right) \quad . \tag{13}$$

Here, all terms are time-dependent. Accordingly, the first order average Hamiltonian vanishes

$$\bar{\hat{\mathcal{H}}}^{\prime\prime(1)} = 0 \quad . \tag{14}$$

It is instructive to look at the second order contribution, which amounts to

$$\bar{\hat{\mathcal{H}}}^{\prime\prime(2)} = \frac{\Omega_S^2}{2\omega_1}\hat{S}_x \quad . \tag{15}$$

These results can be interpreted in the following way. To a first approximation, the offsets in the rotating frame get averaged out to zero. If this approximation is good, then electrons with different resonance frequencies in the rotating frame have the same resonance frequency in the nutating frame. They become equivalent under the spin-lock. As a second approximation, there is a correction that scales with Ω_S^2/ω_1, and this correction acts along the spin-lock axis of the nutating frame. It depends on the bare-spin resonance offset, Ω_S, and it will thus be different for electrons with different bare-spin resonance frequencies. If the bare-spin resonance offset becomes comparable to the Rabi frequency, it is no longer permissible to neglect higher-order terms, and it is better to use an interaction frame with $\Omega_S\hat{S}_z + \omega_1\hat{S}_x$. This corresponds to a nutating frame where the axis of rotation is neither along z nor along x, but somewhere in between. However, now the frame transformation depends on the bare-spin resonance frequency, *i.e.*, on a parameter of the spin system rather than only on parameters chosen by the experimenter and being the same for all spins.

S.1.3.1 Hyperfine decoupling and NOVEL

The Hamiltonian for a single electron coupled to a single nucleus in the electron rotating frame is given by

$$\hat{\mathcal{H}}'_{\text{e-n}} = \hat{S}_z\left(A_{xz}\hat{I}_x + A_{yz}\hat{I}_y + A_{zz}\hat{I}_z\right) + \omega_I\hat{I}_z \quad . \tag{16}$$

An interaction frame transformation with $\omega_1\hat{S}_x$ leads to

$$\begin{aligned}\hat{\mathcal{H}}''_{\text{e-n}} = &\left(\cos(\omega_1 t)\hat{S}_z + \sin(\omega_1 t)\hat{S}_y\right)\\ &\cdot\left(A_{xz}\hat{I}_x + A_{yz}\hat{I}_y + A_{zz}\hat{I}_z\right) + \omega_I\hat{I}_z \quad .\end{aligned} \tag{17}$$

Again, all terms are time-dependent and the first order average Hamiltonian vanishes. If the dominant electron dephasing mechanism relies on the hyperfine coupling, then the dephasing during irradiation should be strongly reduced.

There is, however, a hidden complication, if $\omega_1 \approx \omega_I$. This is best seen by going into the nuclear

rotating frame, *i.e.* the interaction frame with $\omega_I \hat{I}_z$. This leads to

$$\begin{aligned}\hat{\mathcal{H}}''_{\text{e-n}} = &\left(\cos(\omega_1 t)\hat{S}_z + \sin(\omega_1 t)\hat{S}_y\right) \\ &\cdot \left[A_{xz}\left(\cos(\omega_I t)\hat{I}_x - \sin(\omega_I t)\hat{I}_y\right)\right. \\ &+ A_{yz}\left(\cos(\omega_I t)\hat{I}_y + \sin(\omega_I t)\hat{I}_x\right) \\ &\left.+ A_{zz}\hat{I}_z\right] \quad . \end{aligned} \tag{18}$$

If ω_1 matches ω_I, some terms proportional to the pseudo-secular couplings, A_{xz} and A_{yz}, become time-independent. Using trigonometric identities and neglecting time-dependent terms, we obtain

$$\begin{aligned}\hat{\mathcal{H}}''_{\text{e-n}} \approx &\frac{1}{2}\left[\hat{S}_y\left(A_{yz}\hat{I}_x - A_{xz}\hat{I}_y\right)\right. \\ &\left.+ \hat{S}_z\left(A_{xz}\hat{I}_x + A_{yz}\hat{I}_y\right)\right] \quad . \end{aligned} \tag{19}$$

This Hamiltonian generates nuclear polarization ($\hat{I}_z$) from electron coherence ($\hat{S}_x$) and is thus a mechanism for dynamic nuclear polarization (DNP). The matching condition $\omega_1 = \omega_I$ is called the NOVEL condition[2]. In order to avoid magnetization loss, microwave field strengths close to the NOVEL condition should be avoided unless such polarization transfer is intended.

S.1.3.2 Qualitative discussion of electron dephasing in a nuclear spin bath

Let us look at an electron spin in a bath of nuclei. For simplicity and illustration, we only consider one electron and two nuclei. We assume that the electron is only coupled to nucleus one, we neglect the pseudosecular components of the hyperfine coupling and we do include dipole-dipole coupling between the two nuclei. The Hamiltonian in the electron rotating frame thus reads

$$\hat{\mathcal{H}}' = A_{zz}\hat{S}_z\hat{I}_z + \omega_{12}\left(\hat{I}_{1z}\hat{I}_{2z} - \frac{1}{2}\left(\hat{I}_{1x}\hat{I}_{2x} + \hat{I}_{1y}\hat{I}_{2y}\right)\right) \quad , \tag{20}$$

where ω_{12} is the dipolar coupling constant of the two nuclei (and thus depends on the distance between the nuclei and on their gyromagnetic ratios). Let us assume that we created electron coherence along x' and that it further evolves under the sequence $\tau - (\pi)_y - \tau$. If $\omega_{12} = 0$, the π-pulse completely refocuses the hyperfine coupling, and we end up with $-\hat{S}_{x'}$ after the second delay. However, as the flip-flop terms in the nuclear-nuclear coupling Hamiltonian do not commute with the other terms, for $\omega_{12} \neq 0$ evolution generates two- and three-spin terms of the form $\hat{S}_y\hat{I}_{1x}\hat{I}_{2y}$ (among others). The full expression is rather large and does not provide much insight. However, one easily recognizes that these terms are not refocused by a microwave π-pulse acting on the electron spin. Since the terms are not refocused, the amplitude of the electron coherence must necessarily be reduced. Note that this effect is completely coherent. It does not rely on stochastic flips of the nuclear spins. Extending the argument to a large number of nuclear spins with a distribution of hyperfine and nuclear-nuclear couplings, one expects an apparent decay instead of oscillations. A demonstration by numerical simulations would be computationally expensive, as matrix size grows exponentially with the number of spins. Such computations are beyond the scope of this paper.

Note, however, that a spin-lock that is much stronger than the hyperfine coupling averages said coupling. The nuclear-nuclear coupling can then be neglected because it commutes with all the remaining terms that contain electron operators. In other words, a sufficiently strong spin lock isolates the electron spin from the nuclear spin bath, unless the NOVEL condition is met.

S.1.3.3 Electron-electron coupling in the nutating frame

The dipolar coupling Hamiltonian between two electron spins in the electron rotating frame is given by

$$\hat{\mathcal{H}}'_{\text{e-e,dip}} = \omega_{\text{dd}} \left(\hat{S}_{1z}\hat{S}_{2z} - \frac{1}{2}\left(\hat{S}_{1x}\hat{S}_{2x} + \hat{S}_{1y}\hat{S}_{2y}\right)\right) \quad , \tag{21}$$

as already mentioned in the main text. The situation of strong irradiation of *both* spins is well pictured in a nutating frame obtained by transformation with $\omega_1(\hat{S}_{1x} + \hat{S}_{2x})$. This leads to

$$\begin{aligned}\hat{\mathcal{H}}''_{\text{e-e,dip}} = \omega_{\text{dd}} \big[&(c\hat{S}_{1z} + s\hat{S}_{1y})(c\hat{S}_{2z} + s\hat{S}_{2y}) \\ &-\frac{1}{2}\left(\hat{S}_{1x}\hat{S}_{2x} + (c\hat{S}_{1y} - s\hat{S}_{1z})(c\hat{S}_{2y} - s\hat{S}_{2z})\right)\Big]\end{aligned} \tag{22}$$

with

$$\begin{aligned} c &= \cos(\omega_1 t) \\ s &= \sin(\omega_1 t) \quad . \end{aligned} \tag{23}$$

Using the first order average Hamiltonian approximation and the integrals

$$\frac{1}{\tau_c}\int_0^{\tau_c} c \cdot s \, \mathrm{d}t = 0 \tag{24}$$

$$\frac{1}{\tau_c}\int_0^{\tau_c} c^2 \mathrm{d}t = \frac{1}{\tau_c}\int_0^{\tau_c} s^2 \mathrm{d}t = 1/2 \tag{25}$$

$$\tag{26}$$

we obtain the result shown in the main text

$$\begin{aligned}\hat{\mathcal{H}}''_{\text{e-e,dip}} &\approx \omega_{\text{dd}} \left[\frac{1}{2}\hat{S}_{1z}\hat{S}_{2z} + \frac{1}{2}\hat{S}_{1y}\hat{S}_{2y}\right. \\ &\left. -\frac{1}{2}\left(\hat{S}_{1x}\hat{S}_{2x} + \frac{1}{2}\hat{S}_{1y}\hat{S}_{2y} + \frac{1}{2}\hat{S}_{1z}\hat{S}_{2z}\right)\right] \\ &= -\frac{\omega_{\text{dd}}}{2}\left[\hat{S}_{1x}\hat{S}_{2x} - \frac{1}{2}\left(\hat{S}_{1z}\hat{S}_{2z} + \hat{S}_{1y}\hat{S}_{2y}\right)\right]\end{aligned} \tag{27}$$

Note that the simplification leading to this result crucially depends on the condition that both spins are irradiated with the same strength and that the irradiation is stronger than the difference in rotating frame offsets. If the difference in offsets is larger than the dipolar coupling or the Rabi frequency,

$\Delta\Omega > \omega_1, \omega_{dd}$, then the pseudosecular terms in Eq. (21) are already averaged in the doubly rotating frame (meaning that the frames for the two electrons rotate with different frequencies). If only one spin is irradiated, the average dipole-dipole coupling Hamiltonian will vanish. However, if the two spins were irradiated separately with two different frequencies and the same Rabi frequency, part of the Hamiltonian would again be time-independent. This is a situation very similar to Hartmann-Hahn cross-polarization in solid-state NMR.

Regarding the exchange coupling, one can simply argue that it involves a scalar product of spin operators. The scalar product is invariant under frame transformations. However, this statement is slightly dubious because the scalar product of spin operators connects two different spin spaces and may no longer be invariant if the transformations of the two frames differ. Therefore, depending on the irradiation scheme the exchange coupling is not trivially the same between dressed spins as between bare spins. Here, we show explicitly that the exchange coupling is invariant if the same frame transformation is applied to both spins. For an exchange coupling Hamiltonian given by

$$\begin{aligned}\hat{\mathcal{H}}'_{\text{e-e,J}} &= J\left(\hat{\vec{S}}_1 \cdot \hat{\vec{S}}_2\right) \\ &= J\left(\hat{S}_{1x}\hat{S}_{2x} + \hat{S}_{1y'}\hat{S}_y + \hat{S}_{1z}\hat{S}_{2z}\right) \quad , \end{aligned} \tag{28}$$

we employ an interaction frame transformation with $\omega_1(\hat{S}_{1x} + \hat{S}_{2x})$, leading to

$$\begin{aligned}\hat{\mathcal{H}}''_{\text{e-e,J}} &= J\,(\hat{S}_{1x}\hat{S}_{2x} \\ &\quad + (c\hat{S}_{1y} - s\hat{S}_{1z})(c\hat{S}_{2y} - s\hat{S}_{2z}) \\ &\quad + (c\hat{S}_{1z} + s\hat{S}_{1y})(c\hat{S}_{2z} + s\hat{S}_{2y})) \\ &= J\,(\hat{S}_{1x}\hat{S}_{2x} + \hat{S}_{1y}\hat{S}_{2y} + \hat{S}_{1z}\hat{S}_{2z}) \quad . \end{aligned} \tag{29}$$

which is the same as before the interaction frame transformation.

S.1.3.4 Details on the dressed spin echo

Here we explicitly show some more details regarding the dressed spin echo sequence. We assume that the electron spins as well as the spin-lock are along the x' axis. The density operator in the usual rotating frame is then described by

$$\hat{\sigma}'_1 = \hat{S}_{1x} + \hat{S}_{2x} \quad . \tag{30}$$

The Hamiltonian describing the microwave irradiation in the rotating frame is given by

$$\hat{\mathcal{H}}'_{\text{mw}} = \omega_1 \left(\cos\left(\phi_{\text{mw}}(t)\right)\hat{F}_x + \sin\left(\phi_{\text{mw}}(t)\right)\hat{F}_y\right) \quad , \tag{31}$$

with $\hat{F}_x = \hat{S}_{1x} + \hat{S}_{2x}$. The above expression, in the absence of any phase-modulation ($\phi_{\text{mw}}(t) = 0$), reduces simply to

$$\hat{\mathcal{H}}'_{\text{mw}} = \omega_1 \hat{F}_x \quad . \tag{32}$$

As long as the spins and the spin-lock field point along the same direction, nothing happens (apart from relaxation, which is not treated in this formalism). This is even true if we include the dipolar coupling, because again, the sum of polarization does not evolve under the dipolar coupling Hamiltonian.

In order to describe a phase pulse in the rotating frame, we would need to use the Hamiltonian in Eq. (31). The corresponding propagator is given by

$$\hat{U} = \hat{T} \exp\left(-i \int_0^{t_p} \hat{\mathcal{H}}'_{\mathrm{mw}}(t) \mathrm{d}t \right) \tag{33}$$

where $\hat{T}$ is the Dyson time ordering operator. This integral is more of a formality, because it is usually not evaluated this way. Numerically, one can calculate the propagator by time-slicing, *i.e.* by evaluating the time-dependent Hamiltonian and the corresponding propagator for short time steps and calculating the integral by multiplying propagators of the small time steps in the correct order. However, it is much easier to describe a phase pulse in the nutating frame! In this frame, the density matrix above is still given by

$$\hat{\sigma}''_1 = \hat{S}_{1x} + \hat{S}_{2x} \quad , \tag{34}$$

but the Hamiltonian, after the rotating wave approximation, reduces to

$$\hat{\mathcal{H}}''_{\mathrm{mw}} = \frac{\omega_1 a_{\mathrm{PM}}}{2} \left(\cos(\phi_{\mathrm{PM}}) \hat{F}_y + \sin(\phi_{\mathrm{PM}}) \hat{F}_z \right) \quad , \tag{35}$$

which for $\phi_{\mathrm{PM}} = \pi$ (arbitrary) reduces to

$$\hat{\mathcal{H}}''_{\mathrm{mw}} = -\frac{\omega_1 a_{\mathrm{PM}}}{2} \hat{F}_y \quad . \tag{36}$$

This expression is time-independent. The corresponding propagator is then given by

$$\hat{U} = \exp\left(i \frac{\omega_1 a_{\mathrm{PM}}}{2} \hat{F}_y t_p \right) \quad . \tag{37}$$

If we choose $\frac{\omega_1 a_{\mathrm{PM}}}{2} \cdot t_p = \pi/2$, we obtain

$$\hat{U} = \exp\left(i \frac{\pi}{2} \hat{F}_y \right) \quad , \tag{38}$$

which corresponds to a $\frac{pi}{2}$ pulse in the nutating frame. Applied to the density matrix before the pulse, we get

$$\hat{\sigma}''_2 = \hat{U} \hat{\sigma}''_1 \hat{U}^\dagger = \hat{S}_{1z} + \hat{S}_{2z} \quad . \tag{39}$$

The last line can be represented in the product operator formalism (POF) by

$$\hat{S}_{1x} + \hat{S}_{2x} \xrightarrow{-\frac{\pi}{2}\hat{F}_y} (\hat{S}_{1z} + \hat{S}_{2z}) \tag{40}$$

Now we explicitly show how this state evolves under the dipolar Hamiltonian in the nutating frame, *i.e.*

$$\hat{S}_{1z} + \hat{S}_{2z} \xrightarrow{-\frac{\omega_{dd}}{2}\left(\hat{S}_{1x}\hat{S}_{2x} - \frac{1}{2}\left(\hat{S}_{1z}\hat{S}_{2z} + \hat{S}_{1y}\hat{S}_{2y}\right)\right)\cdot t} ? \tag{41}$$

It is important to note that all the two-spin operators in the Hamiltonian commute with each other. This means that we can evaluate their influence on the density operator step-by-step in the POF. We also do it for one spin only and then obtain the result of the second spin by changing the corresponding indices.

$$\begin{aligned}
\hat{S}_{1z} &\xrightarrow{-\frac{\omega_{dd}}{2}\left(\hat{S}_{1x}\hat{S}_{2x}\right)\cdot t} \cos(\frac{\omega_{dd}}{4}t)\hat{S}_{1z} + \sin(\frac{\omega_{dd}}{4}t)\hat{S}_{1y}\hat{S}_{2x} \\
&\xrightarrow{+\frac{\omega_{dd}}{4}\left(\hat{S}_{1y}\hat{S}_{2y} + \hat{S}_{1z}\hat{S}_{2z}\right)\cdot t} \cos(\frac{\omega_{dd}}{4}t)\left[\cos(\frac{\omega_{dd}}{8}t)\hat{S}_{1z} + \sin(\frac{\omega_{dd}}{8}t)\hat{S}_{1x}\hat{S}_{2z}\right] \\
&\quad + \sin(\frac{\omega_{dd}}{4}t)\left[\cos(\frac{\omega_{dd}}{8}t)\hat{S}_{1y}\hat{S}_{2x} - \sin(\frac{\omega_{dd}}{8}t)\hat{S}_{2z}\right]
\end{aligned} \tag{42}$$

Including the result for the second spin, and only keeping terms proportional to $\hat{S}_{1z} + \hat{S}_{2z}$ gives the signal

$$\begin{aligned}
s(t) &= \cos(\frac{\omega_{dd}}{4}t)\cos(\frac{\omega_{dd}}{8}t) - \sin(\frac{\omega_{dd}}{4}t)\sin(\frac{\omega_{dd}}{8}t) \\
&\equiv \frac{1}{2}\left(\cos(\frac{3}{8}\omega_{dd}t) + \cos(\frac{1}{8}\omega_{dd}t) + \cos(\frac{3}{8}\omega_{dd}t) - \cos(\frac{1}{8}\omega_{dd}t\right) \\
&\equiv \cos(\frac{3}{8}\omega_{dd}t)
\end{aligned} \tag{43}$$

Note that in the main text, we display the echo intensity as a function of τ_1 . The effective dipolar evolution time is $2 \cdot \tau_1$, leading to

$$s(t) = \cos(\frac{3}{4}\omega_{dd}\tau_1) \tag{44}$$

S.2 Setting up the dressed spin echo sequence

Here we give a detailed account of the measurement setup for dressed pulse sequences. We assume that the sample is in the spectrometer at the correct temperature and field and that you are able to get an echo.

1. **Set up $\pi/2$ and π pulse lengths** by maximizing the echo amplitude of a Hahn echo where the second pulse is twice as long as the first one. This step seems trivial, but it already suffers from some complications in the case of dipolar coupled trityls, which are seen in the following Figure S1. Clearly, there are two close lying local maxima, which is not compatible with the behavior of a simple spin-1/2 system. The local maxima are due to the small ratio of spectral width compared to the dipolar coupling, and the exact curve depends on the value of the interpulse delay. Note that for the dressed spin sequences, one generally prefers to choose this interpulse delay for the readout as short as possible. A similar observation was reported by Meyer *et al.* [3]

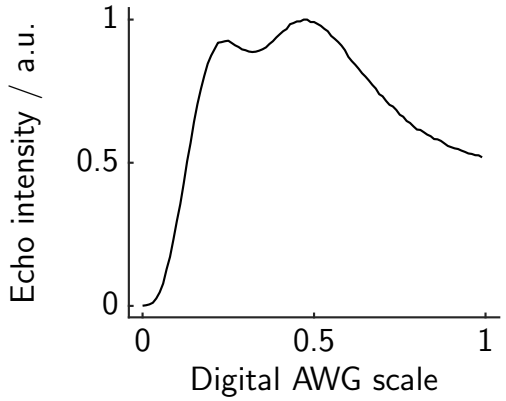

Fig. S1: Echo intensity of a 4/8ns echo as a function of the digital scale of our AWG. (Bis-trityl **1**). Note that starting from around 0.3, the saturation of the TWT becomes significant.

2. **Set up the optimal phase of the spin-lock** with a sequence $\pi/2 - Lock - \tau - \pi - \tau$- echo. In principle, this should not be necessary when using an AWG. In fact, we checked that the phase cycling in our setup works nearly perfectly when simply programming the phases. Additionally, in a two-pulse echo, the phase of the signal perfectly follows the expected phase shift of the coherence order pathway. If this is the case, one would expect that one could simply apply the spin-lock pulse at 90 degrees to the $\pi/2$ pulse, but experimentally, we observe that this is not the case, see Fig. S2. We suspect that phase transients of the pulses due to the resonator are responsible for this behavior.

3. **Measure** $T_{1\rho}$ with the sequence $\pi/2 - Lock - \tau - \pi - \tau$ -echo (SL + echo) with variable length of the spin-lock pulse. Note that a spin-locked echo ($\pi/2 - \tau - Lock - \tau$ - echo, SLE) gives very different results in the case of trityl radicals at low temperatures, see the following Fig. S3. Note also that in the case of the SLE, the decay depends on the interpulse delay. Curiously, one can again see that the maximal echo intensity is not achieved when the spin-lock pulse corresponds to a π pulse, but when it corresponds to a $\pi/2$ or $3\pi/2$ pulse. The red traces in Fig.

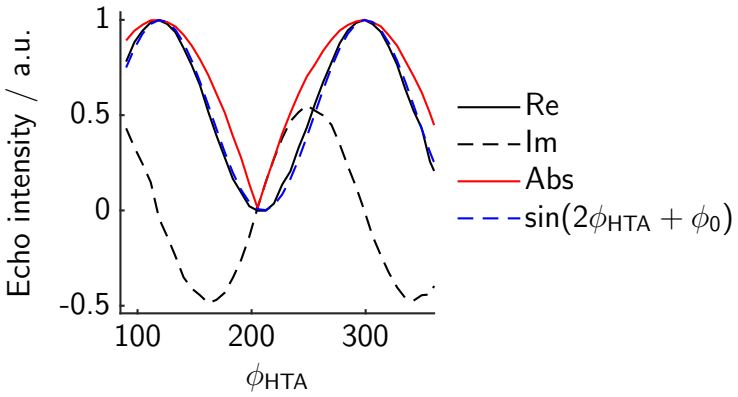

Fig. S2: Echo intensity after a sequence $\pi/2 - Lock - \tau - \pi - \tau$- echo as a function of the digital phase of the spin-lock pulse relative to the first pulse. The length of the spin-lock pulse was $5\mu s$. The highest expected absolute intensity of the echo is at around 120 degrees, while one would expect it around 90 degrees.

S3 correspond to a nutation of the second pulse. Obviously, not only the fundamental oscillation with the Rabi frequency of slightly more than 100 MHz is present, but also an oscillation which is twice as fast. This is due to the fact that a significant part of the echo reduction of the two-pulse echo is due to the dipolar coupling, which is refocused by a solid echo, not a Hahn echo. The solid echo requires a $\pi/2$ pulse. Note however, that the solid echo does not fully refocus the dipolar coupling in the presence of significant offsets compared to the interpulse delay.

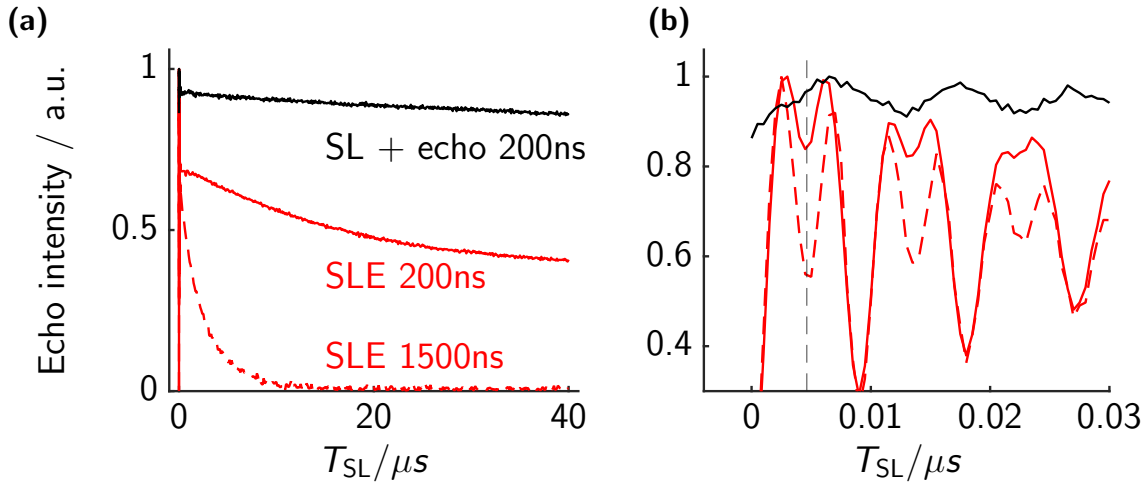

Fig. S3: Measurement of $T_{1\rho}$ with different sequences and different settings. See main text for more details. **(b)** is a zoom of **(a)**.

4. **Record a frequency-stepped dressed spin resonance spectrum.** In order to set the frequency of the phase-modulation, we need to know the Rabi frequency of the spin-lock pulse. It is also useful to know the distribution of the Rabi frequency. One possibility to obtain this information is to use the basic sequence introduced in the main text, but with only a single period of phase-modulation. The amplitude of the phase-modulation should be rather small (*e.g.* 0.02 radians), and the pulse should be rather long (*e.g.* 1 μs.) in order to avoid significant broadening. The

frequency of the phase-modulation is then stepped, and the echo intensity recorded. This is shown in black in Fig. S4. As a comparison, we also show the Fourier transform of a simple nutation experiment in red. The frequency of the phase-modulation for all successive steps was then set to the maximum of the dressed spin resonance spectrum.

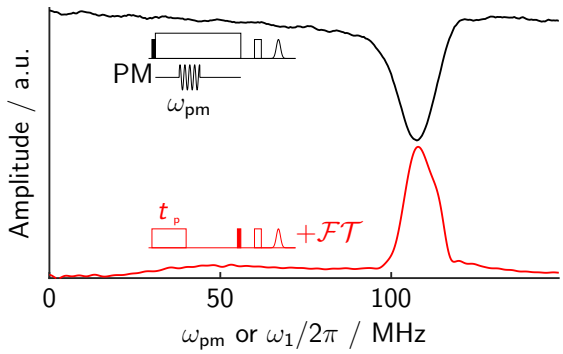

Fig. S4: Frequency-stepped dressed-spin resonance spectrum (black, $a_{pm} = 0.02$, phase pulse length 1 μs). And Fourier transform of a nutation experiment at full power (red). Insets show the pulse sequences. PM denotes the phase modulation during the spin-lock, not an additional channel. Based on this spectrum, a PM frequency of $\omega_{PM}/(2\pi)$ =108 MHz was chosen.

5. **Set up the phase-modulation amplitude and phase-pulse length** Now that the frequency of the phase modulation (ω_{PM}) is set, we can setup the phase-pulse amplitude and length. We can do this by using the same sequence as in the main text, but with only one phase-pulse with fixed modulation frequency. By changing the length of the phase-modulation pulse one obtains a nutation curve in the nutating frame. Fig. S5 shows such nutation curves for $a_{PM} = 0.2$ (grey and black) and $a_{PM} = 0.3$ (red and light red). Interestingly, one can see an overlaid oscillation, which depends on the phase of the phase modulation (ϕ_2). This additional oscillation is due to the breakdown of the rotating wave approximation in the nutating frame and becomes more pronounced with larger phase-modulation intensity. In this case we used the minimum of the phase-pulse nutation curve as a dressed π-pulse length (around 43 ns for $a_{PM} = 0.3$).

6. **Set up the timings for the dressed echo and check the phase-phase cycling.** The sequence from the main text is repeated here in Fig. S6 (a). The dressed echo cannot be acquired continuously. Therefore, we need to check whether the timings of the sequence are correct. In order to do this, we use a fixed spin-lock length T_{SL}, a fixed τ_0 and τ_1 and changed τ_2 step-by-step. A trace with a two-step phase-cycle of $\phi_1 = [(+)0,(-)180]$ and $\phi_2 = \phi_3 = \phi_4 = 0$ is shown in red in Fig. S6 (b). The highest intensity indicates the dressed echo where $\tau_2 = \tau_1$ (plus the length of the first phase pulse, t_p). In addition, one can clearly see additional, *crossing* echoes, and a "dressed FID" around $\tau_2 = 0$. We realized that the position of these crossing echoes depend on the choice of τ_0. This indicates that there is some dressed coherence present during τ_0. This is not very surprising, because the first $\pi/2$ pulse will never be perfect, and some magnetization will be orthogonal to the effective field of the spin-lock. In order to get rid of these crossing echoes, one can cycle the phase of the phase-pulses ϕ_{2-4} in analogy to a bare spin echo, with the complication that at the beginning of the first dressed pulse (after τ_0),

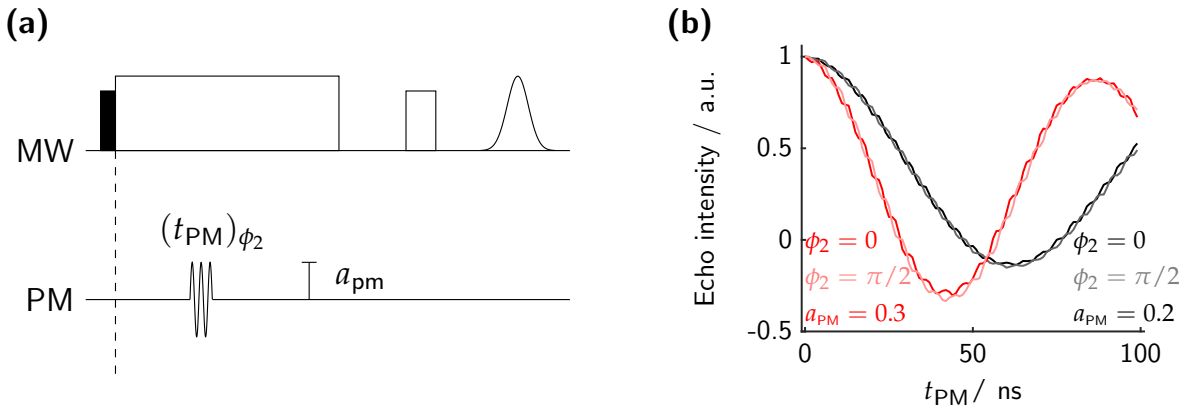

Fig. S5: **(a)** Pulse sequence to set up the dressed pulses. "PM" denotes the phase-modulation during the spin-lock, *not* and additional channel. **(b)** Phase-pulse nutation curves obtained with fixed ω_{PM} but different intensities and phases. The minima of the curves indicate the length of the dressed π pulses for a given intensity a_{PM}.

there is already dressed coherence present. The black trace in Fig. S6 (b) shows the result of the measurement with the 16-step nested phase cycle $\phi_1 = [(+)0, (-)180]$, $\phi_2 = [(+)0, (-)180]$, $\phi_3 = [(+)0, (-)90, (+)180, (-)270]$, which essentially gets rid of all crossing echoes observed in our case. Note that this cycle relies on the fact that dressed coherence decays relatively quickly after the last phase-pulse due to inhomogeneities, and that it does not get refocused after that point. The exact implementation of the phase-modulation and thus the meaning of the phases are given in the next section.

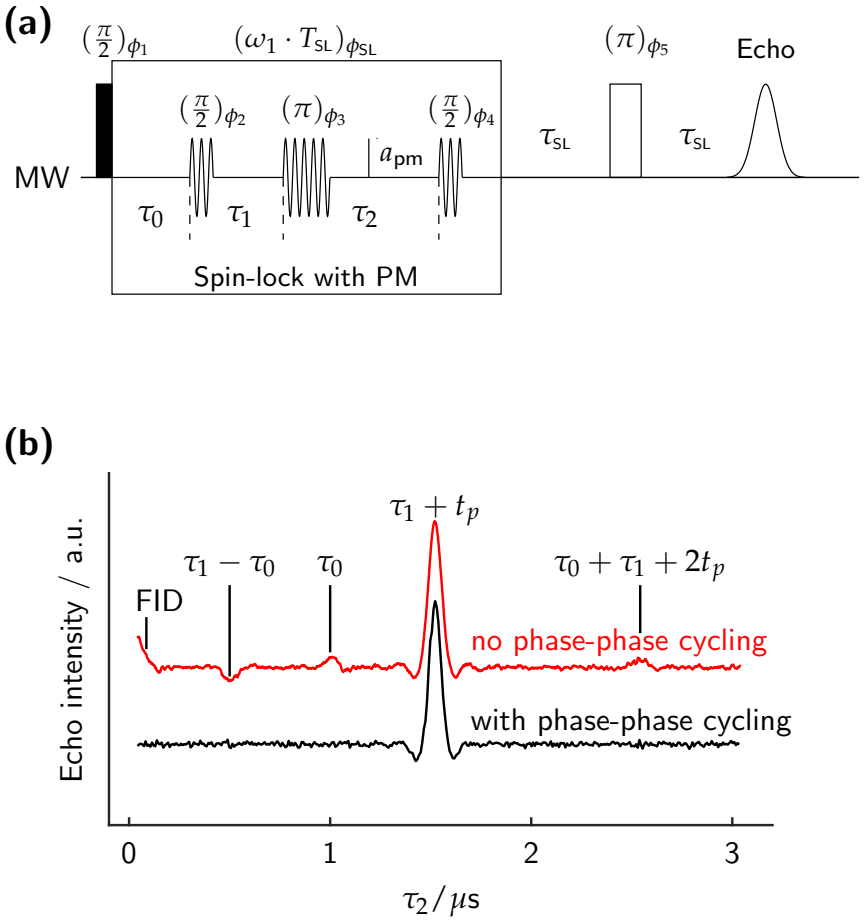

Fig. S6: **(a)** Pulse sequence of the dressed spin echo. **(b)** Dressed echo with fixed τ_0=1μs and τ_1=1.5μs and variable τ_2. Red: $\phi_1 = [(+)0, (-)180]$. Clear crossing echoes are visible. Black: Nested cycle $\phi_1 = [(+)0, (-)180]$, $\phi_2 = [(+)0, (-)180]$, $\phi_3 = [(+)0, (-)90, (+)180, (-)270]$. No crossing echoes visible anymore.

S.3 Implementation details

On our homebuilt AWG based spectrometer, the actual pulse waveform that reaches the sample is generated by IQ-mixing the AWG waveform (IF) with a local oscillator (LO). As an example, we use a Q-band phase-modulated pulse. The LO in this case is around 33.3 GHz. The center frequency of the pulse generated by the AWG is always around 1.5 GHz in our setup. This leads to a final pulse frequency of 33.3+1.5 = 34.8 GHz that reaches the resonator and the spins, as seen in Fig. 3(a), 4(a) and 5(a) in the main text. Apart from the constant value of around 1.5 GHz, we do not use any frequency modulation (FM) in this work ($FM(t) = 1.5$ GHz). The amplitude is also constant during the spin-lock. So let us look now at the phase modulation (PM), which is illustrated in Fig. S7 in red. At most times during the spin-lock, there is no phase modulation. But during the "phase pulses", we turn on the sinusoidal PM. It is best to think about these phase pulses in relation to a hypothetical "carrier". The frequency of this carrier is the dressed spin resonance frequency $\omega_{\mathrm{PM}} \approx \omega_1$ that we determined before in Fig. S4. The phase of this carrier is arbitrarily set to 0 at the beginning of the spin-lock pulse. In our experiment, all three phase pulses have the same frequency as the carrier, but each phase pulse might be phase shifted. This is seen in the example below. The first pulse has a phase $\phi_2 = 0$, which means that the phase is the same for the hypothetical carrier and the phase pulse. The second phase pulse is phase shifted by $\phi_3 = \pi$, and the third one by $\phi_4 = \pi/2$. By cycling the phases of the phase pulses, we can select certain dressed coherence order pathways, in analogy to the bare spin case. Of course the amplitude of the phase modulation (0.3 rad in the example shown here) as

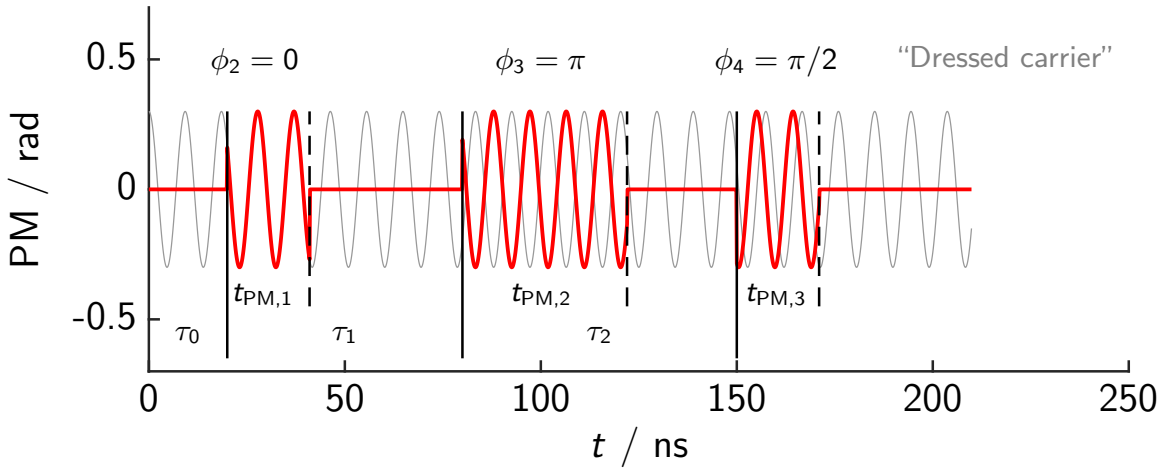

Fig. S7: Illustration of the

well as the length of each phase pulse can be chosen at will. Mathematically, the PM is given by

$$PM(t) = \begin{cases} a_{\mathrm{PM},1}\cos\left(\omega_{\mathrm{PM}}t + \phi_2\right) & \text{for } \tau_0 < t < \tau_0 + t_{\mathrm{PM},1} \\ a_{\mathrm{PM},2}\cos\left(\omega_{\mathrm{PM}}t + \phi_3\right) & \text{for } (\tau_0 + \tau_1) < t < (\tau_0 + \tau_1 + t_{\mathrm{PM},2}) \\ a_{\mathrm{PM},3}\cos\left(\omega_{\mathrm{PM}}t + \phi_4\right) & \text{for } (\tau_0 + \tau_1 + \tau_2) < t < (\tau_0 + \tau_1 + \tau_2 + t_{\mathrm{PM},3}) \\ 0 & \text{otherwise} \end{cases} \tag{45}$$

The total final spin-lock waveform generated by the two channels of the AWG (real and imaginary) is then given by

$$f(t) = AM(t) \cdot \left[\cos\left(2\pi \cdot \int_0^t FM(\tau)\mathrm{d}\tau + PM(t) + \phi_{\mathrm{SL}} \right) + i \sin\left(2\pi \cdot \int_0^t FM(\tau)\mathrm{d}\tau + PM(t) + \phi_{\mathrm{SL}} \right] \right) \quad , \tag{46}$$

where ϕ_{SL} is the overall phase of the spin-lock pulse. We omitted the possible corrections for phase and amplitude for the real and imaginary part.

S.4 Additional experimental data

S.4.1 Dipolar echo envelope modulation: Influence of pulse length

As mentioned in the main text, the dipolar coupling is already visible in the normal Hahn echo decay. Fig. S8 shows these echo decays for the two different bis-trityl compounds, and with different pulse lengths. For both bis-trityls, we see and additional oscillation when very short pulses (4/8 ns) are used. With 100/200 ns pulses, the modulation intensity is reduced. In the case of bis-trityl **2** (5.3 nm) and 4/8 ns pulses, the echo modulation even crosses zero. The presence of these oscillations complicates the analysis of the relaxation data.

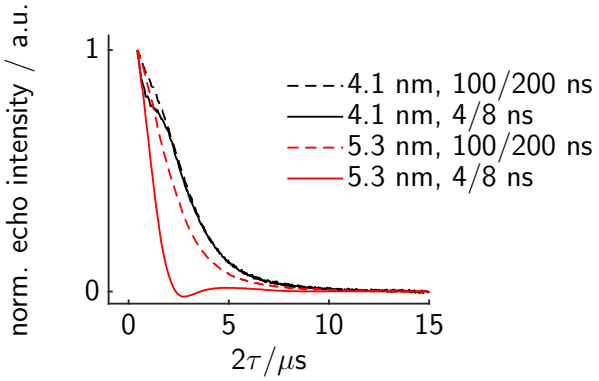

Fig. S8: Hahn echo decay for bis-trityl **1** (4.1 nm) and bis-trityl **2** (5.3 nm) acquired with different pulse lengths. The oscillations are due to the dipolar coupling.

S.4.2 Solvent deuteration: dOTP *vs* OTP

We measured the Hahn echo decay of bis-trityl **1** in *ortho*-terphenyl (OTP) and its deuterated variant (dOTP). Surprisingly, we observed no difference between the two, see Fig. S9. Most likely, the protons in the trityl itself are responsible for the relaxation. Unfortunately, we do not (yet) have the fully deuterated variants of the used trityl moieties in order to test this hypothesis.

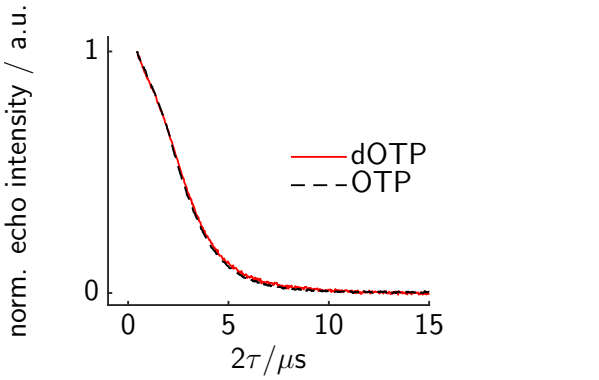

Fig. S9: Hahn echo decay of bis-trityl **1** acuqired with 100/200 ns pulses with OTP and dOTP as solvents. No significant difference can be observed between the two.

S.4.3 SIFTER data for bis-trityls 1 and 2

The SIFTER traces for bis-trityls **1** and **2** and corresponding distance distributions including a sensitvity analysis regarding the background and additional noise are shown in Fig. S10. The fitted background was included in the kernel function [1]. The distance distributions show the expected distances of around 4.1 and 5.3 nm. The oscillations in the case of bis-trityl **1** are quite damped compared to other model systems, and also compared to the dressed echo traces shown in the main text. It is possible that the compound shows strong or intermediate coupling effects for some orientations.

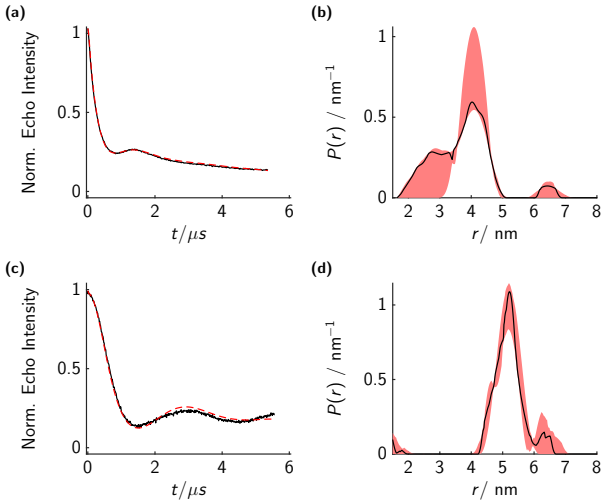

Fig. S10: SIFTER data for bis-trityls **1** and **2**. (**a**) Experimental SIFTER trace (black), symmetrized around the zero-time. Best fit including background in red. (**b**) Corresponding distance distributions obtained with the DeerLab API (`https://github.com/luisfabib/deerlab`). Black curve shows the median values for the probability densities. Red areas span from the 0.25 to 0.75 quantile.

S.5 Additional data for figures in the main article

Here we give detailed information on each figure. This includes information about raw data and processing scripts which are deposited online with a permanent DOI: `10.5281/zenodo.3703053`. Since our home-built spectrometer is run *via* MATLAB© (The MathWorks, Inc), even the raw data are stored in `.mat` files. Some scripts use functions from *EasySpin*[4]. Since *EasySpin*, written in MATLAB, is the most widely used simulation library in the EPR community, we believe that a majority of readers will be able to read and run the scripts we provide. Note that the `.mat` files can also be read into the free software R, with the help of the library 'R.matlab' (https://cran.r-project.org/web/packages/R.matlab/).

Fig. 3 (a)

Q-Band chirp echo Fourier transform EPR spectrum of mono-trityl **7**. 200 μM in dOTP. 6 μl of the solution in a 1.6 mm outer diameter tube. Temperature: 50 K. Pulse sequence: 200/100ns two-pulse chirp echo. Linear chirp pulses with total sweep width of 300 MHz, centered at the center of the resonator (34.8 GHz) and 20 ns rise time were used. The FM function was adjusted to compensate the resonator profile. Interpulse delay 2 μs (start-to-start of pulses). A symmetric 3.6 μs Chebyshev window with 100 dB relative sidelobe attenuation was applied to the digitally down-converted echo. A Fourier transform then yielded the spectrum. Magnetic field: 1241.4 mT (calibrated with DPPH). Shot repetition time 10 ms. 100 shots. 10 averages. $[(+)0,(-)180]$ phase cycle for the first pulse.
Raw data and processing scripts: Matlab processing and simulation: `spectrum_monomer.m`
raw file: `20191106_1239_chirp_echo_dummy.mat`

Fig. 3 (b)

Relaxation measurements for mono-trityl **7**. 200 μM in dOTP. 6 μl of the solution in a 1.6 mm outer diameter tube. Temperature: 50 K. Magnetic field: 1241.4 mT.
T_m measurement: Two-pulse echo ($\pi/2-\tau-\pi-\tau-$ echo) with 100/200 ns pulses. $[(+)0,(-)180]$ phase cycle for the first pulse. Inter-pulse delay varied from 200 ns to 16552 ns in steps of 32 ns (512 points in total). Note that the trace was to long and was thus cut for processing and plotting. Shot repetition time 30 ms. 10 shots per point. 1 average.
$T_{1\rho}$ measurement: $\pi/2-$ lock $-\tau-\pi-\tau-$echo. $(\pi/2)/\pi$ =4/8 ns. τ=200 ns. Spin-lock Rabi frequency around 100 MHz. $[(+)0,(-)180]$ phase cycle for the $\pi/2$ pulse, $[(+)0,(+)180]$ phase cycle for the π pulse. Fixed phase for the spin-lock, but always orthogonal to the first pulse. Spin-lock length varied from 0 ns to 100 ns in steps of 0.5 ns, and from 200 ns to 40 μs in steps of 100 ns (600 points in total). Shot repetition time 30 ms. 5 shots per point. 1 average.
$T_{2\rho}$ measurement: Dressed spin echo, see previous sections for detailed definitions. Dressed $(\pi/2)/\pi$ pulse lengths 21/42 ns, with an amplitude of 0.3 rad. Total spin-lock length 35 μs. Modulation frequency of 99 MHz. τ_0 =2 μs, τ_1 varied from 22 ns to 14390 ns in steps of 32 ns (450 points in total). Phase cycle and phase-phase cycle as introduced above. Shot repetition time 30 ms. 1 shot per point. 300 averages (overkill, was simply overnight). All other parameters as for the $T_{1\rho}$ measurement.
Raw data and processing scripts:

Matlab processing and simulation: `relaxation_monomers.m`
raw file T_m measurement: `20200203_1538_2pecho_ESEEM.mat`
raw file $T_{1\rho}$ measurement: `20200203_1549_spin_locked_echo_t1rho.mat`
raw file $T_{2\rho}$ measurement: `20200203_1700_spin_locked_phase_echo_mod`

Fig. 4 (a)

Q-Band chirp echo Fourier transform EPR spectrum of bis-trityl **1**. 100 μM in dOTP. 6 μl of the solution in a 1.6 mm outer diameter tube. Temperature: 50 K. Pulse sequence: 200/100ns two-pulse chirp echo. Linear chirp pulses with total sweep width of 300 MHz, centered at the center of the resonator (34.8 GHz) and 20 ns rise time were used. The FM function was adjusted to compensate the resonator profile. Interpulse delay 950 ns (start-to-start of pulses). A symmetric 3.6 μs Chebyshev window with 100 dB relative sidelobe attenuation was applied to the digitally down-converted echo. A Fourier transform then yielded the spectrum. Magnetic field: 1241.4 mT (calibrated with DPPH). Shot repetition time 10 ms. 100 shots. 1 average. $[(+)0,(-)180]$ phase cycle for the first pulse.
Raw data and processing scripts: Matlab processing and simulation: `spectrum_4p1nm.m`
raw file: `20190729_1134_chirp_echo_dummy.mat`

Fig. 4 (b)

Relaxation measurements for bis-trityl **1**. 100 μM in dOTP. 6 μl of the solution in a 1.6 mm outer diameter tube. Temperature: 50 K. Magnetic field: 1241.4 mT.
T_m measurement: Two-pulse echo ($\pi/2-\tau-\pi-\tau-$ echo) with 100/200 ns pulses. $[(+)0,(-)180]$ phase cycle for the first pulse. Inter-pulse delay varied from 200 ns to 8376 ns in steps of 16 ns (512 points in total). Shot repetition time 30 ms. 10 shots per point. 1 average.
$T_{1\rho}$ measurement: $\pi/2-$lock$-\tau-\pi-\tau-$echo. $(\pi/2)/\pi$ =4/8 ns. τ=200 ns. Spin-lock Rabi frequency around 100 MHz. $[(+)0,(-)180]$ phase cycle for the $\pi/2$ pulse, $[(+)0,(+)180]$ phase cycle for the π pulse. Fixed phase for the spin-lock, but always orthogonal to the first pulse. Spin-lock length varied from 0 ns to 100 ns in steps of 0.5 ns, and from 200 ns to 40 μs in steps of 100 ns (600 points in total). Shot repetition time 30 ms. 5 shots per point. 1 average.
Raw data and processing scripts:
Matlab processing and simulation: `relaxation_4p1nm.m`
raw file T_m measurement: `20191101_1415_2pecho_ESEEM.mat`
raw file $T_{1\rho}$ measurement: `20190819_1706_spin_locked_echo_t1rho.mat`

Fig. 4 (c) and (d)

Dressed echo decay/modulation for bis-trityl **1**. See previous sections for detailed definitions. 100 μM in dOTP. 6 μl of the solution in a 1.6 mm outer diameter tube. Temperature: 50 K. Magnetic field: 1241.4 mT. Dressed $(\pi/2)/\pi$ pulse lengths 21/42 ns, with an amplitude of 0.34 rad. Total spin-lock length 25 μs. Modulation frequency of 108 MHz. τ_0 =1 μs, τ_1 varied from 22 ns to 8997 ns in steps of 25 ns (360 points in total). Phase cycle and phase-phase cycle as introduced above. Shot repetition

time 30 ms. 5 shot per point. 63 average. All other parameters as for the $T_{1\rho}$ measurement. Background correction with a stretched exponential and a Fourier transform gives the spectrum.
Raw data and processing scripts:
Matlab processing and simulation: `dressed_echo_modulation_4p1nm.m`
raw file: `20190820_1736_spin_locked_phase_echo_mod.mat`

Fig. 5 (a)

Q-Band chirp echo Fourier transform EPR spectrum of bis-trityl **2**. 100 μM in dOTP. 6 μl of the solution in a 1.6 mm outer diameter tube. Temperature: 50 K. Pulse sequence: 200/100ns two-pulse chirp echo. Linear chirp pulses with total sweep width of 300 MHz, centered at the center of the resonator (34.8 GHz) and 20 ns rise time were used. The FM function was adjusted to compensate the resonator profile. Interpulse delay 950 ns (start-to-start of pulses). A symmetric 3.6 μs Chebyshev window with 100 dB relative sidelobe attenuation was applied to the digitally down-converted echo. A Fourier transform then yielded the spectrum. Magnetic field: 1241.4 mT (calibrated with DPPH). Shot repetition time 10 ms. 100 shots. 1 average. $[(+)0,(-)180]$ phase cycle for the first pulse.
Raw data and processing scripts: Matlab processing and simulation: `spectrum_5p3.m`
raw file: `20191101_1155_chirp_echo_dummy.mat`

Fig. 5 (b)

Relaxation measurements for bis-trityl **2**. 100 μM in dOTP. 6 μl of the solution in a 1.6 mm outer diameter tube. Temperature: 50 K. Magnetic field: 1241.4 mT.
T_m measurement: Two-pulse echo ($\pi/2-\tau-\pi-\tau-$ echo) with 100/200 ns pulses. $[(+)0,(-)180]$ phase cycle for the first pulse. Inter-pulse delay varied from 200 ns to 8376 ns in steps of 16 ns (512 points in total). Shot repetition time 30 ms. 10 shots per point. 1 average.
$T_{1\rho}$ measurement: $\pi/2-$lock$-\tau-\pi-\tau-$echo. $(\pi/2)/\pi$ =4/8 ns. τ=200 ns. Spin-lock Rabi frequency around 100 MHz. $[(+)0,(-)180]$ phase cycle for the $\pi/2$ pulse, $[(+)0,(+)180]$ phase cycle for the π pulse. Fixed phase for the spin-lock, but always orthogonal to the first pulse. Spin-lock length varied from 0 ns to 100 ns in steps of 0.5 ns, and from 200 ns to 40 μs in steps of 100 ns (600 points in total). Shot repetition time 30 ms. 5 shots per point. 1 average.
Raw data and processing scripts:
Matlab processing and simulation: `relaxation_5p3nm.m`
raw file T_m measurement: `20191101_1336_2pecho_ESEEM.mat`
raw file $T_{1\rho}$ measurement: `20191101_1058_spin_locked_echo_t1rho.mat`

Fig. 5 (c) and (d)

Dressed echo decay/modulation for bis-trityl **2**. See previous sections for detailed definitions. 100 μM in dOTP. 6 μl of the solution in a 1.6 mm outer diameter tube. Temperature: 50 K. Magnetic field: 1241.4 mT. Dressed $(\pi/2)/\pi$ pulse lengths 22/44 ns, with an amplitude of 0.3 rad. Total spin-lock length 35 μs. Modulation frequency of 108 MHz. τ_0 =1 μs, τ_1 varied from 22 ns to 14390 ns in steps

of 32 ns (450 points in total). Phase cycle and phase-phase cycle as introduced above. Shot repetition time 30 ms. 5 shot per point. 56 average. All other parameters as for the $T_{1\rho}$ measurement.
Background correction with a stretched exponential and a Fourier transform gives the spectrum.

Raw data and processing scripts:

Matlab processing and simulation: `dressed_echo_modulation_5p3nm.m`
raw file: `20190821_1636_spin_locked_phase_echo_mod.mat`

Fig. 6 (a) to (d): Simulations

The simulation scripts are named *runsim_*.m*. Where the asterisk describes the distance, offset distributions and Rabi frequencies. The actual simulation is done by the function *spinlock.m* . The corresponding plotting scripts are named *plot_*.m*. (But you have to run the simulations first such that the results are saved).

References

1 Fábregas Ibáñez, L. and Jeschke, G.: Optimal background treatment in dipolar spectroscopy, Phys. Chem. Chem. Phys., 22, 1855–1868, https://doi.org/10.1039/C9CP06111H, 2020.

2 Henstra, A., Dirksen, P., Schmidt, J., and Wenckebach, W. T.: Nuclear spin orientation via electron spin locking (NOVEL), Journal of Magnetic Resonance (1969), 77, 389–393, https://doi.org/10.1016/0022-2364(88)90190-4, 1988.

3 Meyer, A., Jassoy, J. J., Spicher, S., Berndhäuser, A., and Schiemann, O.: Performance of PELDOR, RIDME, SIFTER, and DQC in measuring distances in trityl based bi- and triradicals: Exchange coupling, pseudosecular coupling and multi-spin effects, Physical Chemistry Chemical Physics, 20, 13 858–13 869, https://doi.org/10.1039/c8cp01276h, 2018.

4 Stoll, S. and Schweiger, A.: EasySpin, a comprehensive software package for spectral simulation and analysis in EPR, Journal of Magnetic Resonance, 178, 42–55, https://doi.org/10.1016/j.jmr.2005.08.013, 2006.